2018

Degradation of Select Chlorinated Hydrocarbons by (i) Sulfide-Treated Hydrous Ferric Oxide (HFO) and (ii) Hydroxyl Radicals Produced in the Dark by Oxygenation of Sodium Dithionite-Reduced HFO

Dhurba Raj Pandey
Wright State University

DEGRADATION OF SELECT CHLORINATED HYDROCARBONS BY:

(i) SULFIDE-TREATED HYDROUS FERRIC OXIDE (HFO) AND

(ii) HYDROXYL RADICALS PRODUCED IN THE DARK BY OXYGENATION OF

SODIUM DITHIONITE-REDUCED HFO

A thesis submitted in partial fulfillment of the

requirements for the degree of

Master of Science

By

DHURBA RAJ PANDEY

B.S., Tribhuvan University, 2010

M.S., Tribhuvan University, 2014

2018

Wright State University

WRIGHT STATE UNIVERSITY

GRADUATE SCHOOL

July 24, 2018

I HEREBY RECOMMEND THAT THE THESIS PREPARED UNDER MY SUPERVISION BY <u>Dhurba Raj Pandey</u> ENTITLED <u>Degradation of Select Chlorinated Hydrocarbons by (i) Sulfide-Treated Hydrous Ferric Oxide (HFO) and (ii) Hydroxyl Radicals Produced in the Dark by Oxygenation of Sodium Dithionite-Reduced HFO</u> BE ACCEPTED IN PARTIAL FULFILLMENT OF THE REQUIREMENTS FOR THE DEGREE OF <u>Master of Science</u>.

_____
Abinash Agrawal, Ph.D.
Thesis Director

_____
David F. Dominic, Ph.D.
Chair, Department of Earth & Environmental Sciences

Committee on Final Examination:

_____
Abinash Agrawal, Ph.D.

_____
Hailiang Dong, Ph.D.

_____
David Kempisty, Ph.D.

_____
Barry Milligan, Ph.D.
Interim Dean of the Graduate School

ABSTRACT

Pandey, Dhurba Raj. M.S. Department of Earth and Environmental Sciences, Wright State University, 2018. Degradation of Select Chlorinated Hydrocarbons by (i) Sulfide-Treated Hydrous Ferric Oxide (HFO) and (ii) Hydroxyl Radicals Produced in the Dark by Oxygenation of Sodium Dithionite-Reduced HFO

A previous work demonstrated that sulfide-treated iron oxides (goethite, hematite, and magnetite) may not show reductive pathways with carbon tetrachloride (CT) as observed with lab-precipitated iron sulfide. We examined the kinetics and products of reaction of sulfide-treated hydrous ferric oxide (HFO) towards select chlorinated hydrocarbons in batch reactors with HFO: HS^- molar ratio of 1:1.5 at pH 7. CT, 1,1,2-trichlroethane (1,1,2-TeCA), 1,1,1,2-tetrachloroethane (1,1,1,2-TeCA) and 1,1,2,2-tetrachloroethane (1,1,2,2-TeCA) showed faster kinetics whereas chloroform (CF) showed slower kinetics. Trichloroethene (TCE) degradation was observed at three pHs: 7, 8 and 10; the loss in reactors were not much different from controls at pH 7, 8 and 10.

The degradation products of 1,1,2-TCA (1,1-DCE, 33%), 1,1,1,2-TeCA (TCE, 29%), and 1,1,2,2-TeCA (TCE~100%) suggest dehydrohalogenation to be the major pathway. The degradation product of CT (4% CF; hydrogenolysis) and 1,1,1,2-TeCA (4% 1,1 DCE; β elimination) shows reduction to be a minor pathway. This suggests that unlike the lab-precipitated FeS, formed by reaction of Fe (II) and HS^-, reduction may not be a major pathway for sulfide-treated HFO.

Recent studies identified a light independent pathway for generation of hydroxyl radicals in which hydroxyl radicals are produced during O_2 reduction by electron donors such as Fe (II) and DOC. Most studies have focused on hydroxyl radical production from reduced structural Fe (II) in clays and sediments. Study of reduced iron oxide in this respect remains largely uninvestigated. In this part of the research, hydrous ferric oxide (HFO) was reduced by sodium dithionite (SD) and the resulting phase was oxygenated in the dark. This bench scale study shows the age of the phase formed by SD reduced HFO did not affect the rates of *cis*-1,2-DCE degradation. k_{obs1} of *cis*-1,2-DCE degradation did not depend on the initial amount of *cis*-1,2-DCE. k_{obs1} of *cis*-1,2-DCE degradation increased non-proportionately with increase in the concentration of dithionite. Effect on *cis*-1,2-DCE degradation rates were investigated at three HFO:SD molar ratios: 9.4:1, 4.7:1 and 2.4:1 (SD concentration is increasing by a factor of ~2 successively); The ratios of k_{obs1} were 1:10.8:13.8 (normalized to k_{obs1} of 9.4:1) for these three ratios respectively indicating a magnitude of order increase between 9.4:1 to 4.7:1 while it increased by 1.27 times between two higher ratios 4.7:1 to 2.4:1.

Observed order of k_{obs1} was :1,1-DCE >TCE > PCE > *cis*-1,2-DCE > *trans*-1,2-DCE and ethene. The reactivity increased with decreasing number of chlorine substituents for 1,1-DCE >TCE> PCE and may be explained based on strong inductive effect exerted by chlorine atoms. Surprisingly, ethene with no chlorine substituents showed the least reactivity. The ratio of rate constants observed are consistent to that observed with hydroxyl radicals generated from other methods. The order for DCE isomers 1,1-DCE> *cis*-1,2-DCE > *trans*-1,2-DCE may be explained based on position of the chlorine substituents.

TABLE OF CONTENTS

LIST OF FIGURES

LIST OF TABLES

ACKNOWLDEGEMENTS

Firstly, I want to express my sincere gratitude to Dr. Abinash Agrawal, my advisor, for introducing me to the fascinating world of iron geochemistry and instilling concepts of redox ladder. I would not have been able to complete my thesis research without his constant guidance, support, and being there whenever I had questions or doubts. I also thank Dr. Dong and Dr. Kempisty for being in my thesis committee.

I am also thankful to Earth and Environmental Science Department for funding my M.S. study at Wright State. I am equally indebted to other professors as well as administrative staff, including Andrea Peterson and Suzanne Semones for their help throughout my time at Wright State University.

I am also thankful to other members in Dr. Agrawal's lab: Adam Burdsall, Jaya Das and Bo Wang for training me in laboratory methods. Particularly, Adam was very helpful in training me with GC and HPLC analyses, Fe oxides synthesis, etc.

I will miss the late night pizza on campus with Dan, and the weekend lunch with Dan, Saiful and John. Finally, I would like to thank my wife for being supportive throughout my study and helping me in chasing my dreams.

CHAPTER 1

DEGRADATION OF SELECT CHLORINATED HYDROCARBONS BY SULFIDE-
TREATED HYDROUS FERRIC OXIDE (HFO)

1.1 BACKGROUND

1.1.1 Groundwater Contamination by Chlorinated Hydrocarbons

Chlorinated hydrocarbons (CHCs), organic compounds with 1-3 carbon atoms
and at least one covalently-bonded chlorine atom (Cwiertny and Scherer, 2010a), were
first produced in the USA in 1906, and their massive industrial usage escalated from
WWII (Pankow and Cherry, 1996). Since then CHCs have been used in variety of
industrial and commercial applications such as degreasing and cleaning, adhesives,
aerosols, industrial solvents and in paint removal (Huang et al., 2014; Pankow and
Cherry, 1996; Wong et al., 2009).

Groundwater contamination by CHCs has been realized as a widespread problem
(Moran, et al., 2007). Some of the common contaminants include carbon tetrachloride
(CT), 1,1,1-trichloroethane (1,1,1-TCA), 1,2- dichloroethane (1,2-DCA), perchloroethene
(PCE), trichloroethene (TCE) and chloroethene (Cwiertny and Scherer, 2010a). As of
July 2017, trichloroethene, tetrachloroethene, chloroethene and dichloromethane were

among the top 20 contaminants with each observed at 1061, 917, 658 and 609 superfund sites respectively (USEPA 2017). Some of the common ways for introduction of CHCs into groundwater include leakage from storage tanks, accidental spillage, and intentional release when open dumping was an accepted disposal method and adverse effects were unknown (Pankow and Cherry, 1996). CHCs often have a specific gravity >1 and they are non-miscible in water and therefore, once released into the subsurface, they travel below the water table and enter fractured rocks and diffuse into clays, and form isolated sources and ganglia, from where they slowly dissolve in groundwater (Zhang et al., 2011).

1.1.2 Chlorinated Hydrocarbons Remediation

In past four decades, considerable efforts have been directed towards remediation of chlorinated hydrocarbons (CHCs) in the groundwater, and consequently, many remediation techniques have been developed. During 1980s and early 1990s, the remediation techniques mainly included excavation and safe disposal of contaminated soil, often referred as "dig-and-dump". Thereafter, methods were developed to extract the contaminated media and remediate it by capture/destruction, often referred to as "pump-and-treat". However, a complete extraction of the contaminants from the impacted subsurface zones was often difficult to achieve using these techniques. After that, *in situ* approaches to degrade the contamination such as *in situ* chemical oxidation (ISCO), *in situ* chemical reduction (ISCR), and bioremediation were developed.

More recently, there is an increased interest in studying natural attenuation (NA) techniques as an alternative strategy for engineered remediation of contaminants owing to

its small financial and environmental footprint (less intrusive). Conceptually, NA pertains to the reduction of contaminants' concentration to acceptable levels by one of the natural processes: dispersion, sorption, volatilization, and degradation by naturally occurring microbial and abiotic reaction (Davis et al., 2003); the first three are nondestructive processes (a phase transfer) while the last two are destructive processes (Wiedmeier et al.,1996).

Biodegradation as a natural attenuation process has been studied extensively. However, the biodegradation of some CHCs such as trichloroethene can produce daughter products, such as dichloroethenes and vinyl chloride, which are more toxic and persistent than the parent compound (He et al., 2010). This limitation of biodegradation has drawn considerable interest towards studying reaction of chlorinated hydrocarbons with specific minerals in the subsurface (e.g., iron sulfide, magnetite, goethite, green rust etc.)

1.1.3 Abiotic Natural Attenuation

Abiotic natural attenuation could be of considerable interest under iron and sulfate reducing conditions, where reduced iron minerals (e.g., magnetite, green rust, iron sulfide) are expected to develop and be stable. Such conditions can develop down gradient from leaky landfills, wetlands, fuel-contaminated sites, and in aquifers with higher influx of organic matter (He et al., 2015; Kennekke and Weber 2003). Sulfate reducing zones are also expected to increase near coastal aquifers with sea level rise due to climate change as sulfate rich seawater encroaches on the land and salt-water intrusion occurs (Kumar, et al., 2018).

Numerous studies (Amir and Lee, 2012; Butler and Hayes, 1998; 1999; 2001; Jeong and Hayes, 2007) have examined the CHC degradation with chemically-precipitated (synthetic) ferrous iron minerals, such as FeS (mackinawite), produced by the homogenous aqueous-phase reaction of Fe(II) and S(II). In a study (Hanoch et al., 2006), CHC degradation has been demonstrated by sulfide-treated iron oxides; while the authors in this study did not clearly establish the mechanism of CT transformation by sulfide-treated iron oxide, it sufficiently demonstrated that hydrogenolysis is not a major mechanism as only a small amount of chloroform was observed (<1%) and no dichloromethane and methane were observed. Hydrogenolysis being a minor pathway in the above study (Hanoch et al., 2006) is contrary to the product distribution with reduced iron minerals such as FeS, magnetite and green rust (Butler and Hayes, 2000; McCormick et al.,2002; Maithreepala and Doong, 2005; O' Loughlin et al., 2003), which mainly demonstrated CT reduction by hydrogenolysis (CF as a major daughter product) as the major pathway. The subsurface reaction of amorphous iron oxide with a plume of aqueous sulfide could be a more realistic representation of what happens in the subsurface.

1.1.4 Sulfate Reducing Zone Geochemistry

In a typical Sulfate Reducing Zone (SRZ), the second most common reducing condition in the subsurface, the sulfate reducing bacteria use sulfate as a terminal electron acceptor that produces bisulfide [HS$^-$] at circumneutral pH (Christensen et al., 2000; Miao et al., 2012) [Equation 1.1].

$$SO_4^{2-} + 9H^+ + 8e^- \rightarrow HS^- + 4H_2O \qquad (1.1)$$
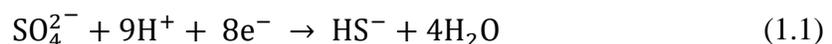
This bisulfide can migrate along the water flow paths and cause reductive dissolution of iron (Fe^{3+}) oxide species in the aquifer matrix to form dissolved Fe^{2+} species (Hanoch et al., 2006). An example of the reductive dissolution of goethite by bisulfide (HS^-) is given below in Equation 1.2a (Pyzik and Sommer, 1981). The dissolved Fe^{2+} can further react with aqueous HS^- or H_2S to form authigenic iron monosulfide (FeS), as in Equation 1.2b (Rickard and Luther, 2007). A similar reaction scheme for hydrous ferric oxide (HFO) can be as written in Equations 1.3a and 1.3b.

$$2FeOOH(s) + HS^- + H_2O \rightarrow 2Fe^{2+} + S^0 + 5OH^- \qquad (1.2.a)$$

$$2Fe^{2+} + 2HS^- \rightarrow 2FeS + 2H^+ \qquad (1.2.b)$$
$$\overline{\phantom{2FeOOH(s) + HS^- + H_2O \rightarrow 2Fe^{2+}}}$$
$$2FeOOH(s) + 3HS^- + H_2O \rightarrow 2FeS + S^0 + 2H_2O + 3OH^- \qquad (1.2)$$

$$2Fe(OH)_3(s) + HS^- \rightarrow 2Fe^{2+} + S^0 + 5OH^- + H_2O \qquad (1.3a)$$

$$2Fe^{2+} + 2HS^- \rightarrow 2FeS + 2H^+ \qquad (1.3b)$$
$$\overline{\phantom{2Fe(OH)_3(s) + HS^- \rightarrow 2Fe^{2+}}}$$
$$2Fe(OH)_3(s) + 3HS^- \rightarrow 2FeS + S^0 + 4OH^- + 2H_2O \qquad (1.3)$$
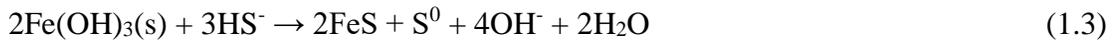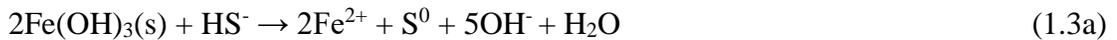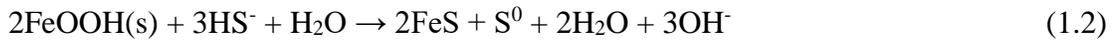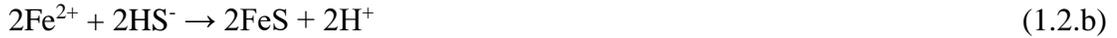
Above equations depict that FeS formation from iron oxide is a two-step process: the first step (reduction/dissolution) requires 1 mole of HS^- to reduce 2 moles of iron oxide, and the second step requires two additional moles of HS^- to precipitate 2 moles of FeS; the stoichiometric ratio for reaction of HS^-/Fe is 1.5:1 (Equations 1.2 and 1.3). A recent study by Kumar et al. (2018) supports the reaction scheme above; at HS^-/Fe ratio ≤ 0.5, they observed only reductive dissolution of iron oxide but no FeS precipitation. However, at HS^-/Fe = 2, Kumar et al. (2018) noted a complete transformation of ferrihydrite to FeS,

and at $HS^-/Fe = 1$, they reported that 50% of ferrihydrite transformed to FeS; however, they did not examine $HS^-/Fe = 1.5$.

1.1.5 Ferrihydrite

Ferrihydrite, loosely termed as hydrous ferric oxide (HFO), is a nanophase and a precursor to other iron oxides such as goethite and hematite, and it is widespread in the natural environment as freshly formed Fe oxide phase. HFO is of considerable interest in biogeochemistry due to its high reactivity and high specific surface area among all iron oxides (Villacis-Garcia et al., 2015; Villalobos and Antelo, 2011). Although N_2-BET measurements of dried HFO samples show a specific surface area (SSA) of 200-300 m^2/g, a theoretical modeling study has argued the SSA of fresh HFO as high as 1250 m^2/g (Villalobos and Antelo, 2011). Such a high SSA at water/mineral interface indicates high potential reactivity for chemicals at the HFO surface. Thus, HFO may have a considerable influence in chemical reactions where they are present, such as in its reaction with aqueous HS^- ions (sulfidation).

1.1.6 Research Objectives

Reduced iron minerals, such as FeS (mackinawite), produced by the homogenous reaction of aqueous Fe(II) and S(II) reagent solutions may not be representative of what can happen in the subsurface. A more realistic scenario could be reaction as aqueous plume of HS^- coming in contact with iron (Fe^{3+}) oxides. This study examines the transformation potential of sulfide-treated HFO towards selected CHCs (CT, CF, 1,1,2-TCA, 1,1,1,2-TeCA, 1,1,2,2-TeCA and TCE). The major objectives of this study were to

investigate: (i) the reaction byproducts and (ii) kinetics of CHC reaction with sulfide-treated HFO.

1.2 MATERIALS AND METHODS

1.2.1 Chemicals

Following chemicals were used as received: carbon tetrachloride (CT, Fisher Scientific, 99.8%) chloroform (CF, Fisher Scientific, 99.8%), dichloromethane (DCM, Fisher Scientific, 99.9%), 1,1,2,2 tetrachloroethane (1,1,2,2-TeCA, Acros Organics, 98.5%), 1,1,1,2-tetrachloroethane (1,1,1,2-TeCA, Sigma-Aldrich, 99%), 1,1,2-trichloroethane (1,1,2-TCA, Sigma-Aldrich, 96%), 1,1,1-trichloroethane (1,1,1-TCA, Sigma-Aldrich, 99%), 1,2-dichloroethane (1,2-DCA, Sigma-Aldrich, 99%), 1,1-dichloroethane (1,1-DCA, Pfaltz and Bauer, 99%), tetrachloroethene (PCE, Sigma-Aldrich, 99.9%), trichloroethene (TCE, Acros Organics, 99%), *cis*-1,2-dichloroethene (*cis*-DCE, Acros Organics, 97%), *trans*-1,2 dichloroethene (*trans*-DCE, Acros Organics, 99%), 1,1-dichloroethene (1,1-DCE, Tokyo Chemical Industries, 99%), and vinyl chloride (VC, Air Liquide, 1,000 ppmv with nitrogen balance). Other used chemicals include ferric chloride hexahydrate (FeCl$_3$.6H$_2$O, ACS grade, Ricca Chemical Company), sodium sulfide nonahydrate (Alfa Aesar, 98%), TAPSO (2 hydroxy-3-[tris (hydroxymethyl)methylamino]-1 propanesulfonic acid, N [tris(hydroxymethyl) methyl]-3-amino-2-hydroxypropanesulfonic acid; Sigma-Aldrich, 99%), sodium hydroxide (NaOH, Fisher Scientific, 99.1%), and high purity gases (CH$_4$, He, N$_2$, H$_2$, air; zero grade; Praxair, Dayton, OH).

1.2.2 Experimental Setup

Nanoscale HFO was synthesized by neutralizing 0.1 M ferric chloride hexahydrate ($FeCl_3.6H_2O$) with 0.3 M NaOH (Zachara et al., 1998). The NaOH solution was added dropwise until the pH of the HFO suspension reached ~7.2-7.3. This HFO was allowed to react overnight on a magnetic stir plate, and then was repeatedly washed with deionized water until the electrical conductivity of the supernatant was less than 250 µS cm^{-1}. The final HFO slurry was made by adding TAPSO buffer solution (pH 7 in all experiments, except in pH 8 and pH 10 experiments for TCE) to obtain a final concentration of 37.5 mM for TAPSO buffer and the desired pH. After transferring 49 mL of 25 mM (1.4 g/L) HFO slurry to borosilicate glass serum bottles (reactors) of 72 mL volume, the reactors were sealed with PTFE-lined butyl rubber stopper and aluminum crimp. The reactors were then deoxygenated by bubbling with a gentle stream of high-purity N_2 gas through a stainless-steel needle piercing through the stopper for 20 mins. Each experiment had triplicate reactors to validate the reproducibility of the results.

Aqueous sulfide reagent was prepared by dissolving sodium sulfide ($Na_2S.9H_2O$) solid in deoxygenated deionized water, and it was added to the deoxygenated HFO reactors slowly by a N_2-purged syringe, which resulted in the brown HFO solids to become a black precipitate. The reactors were then equilibrated on rotatory shakers overnight. Two control reactors were prepared along with triplicate reactors in each experiment, including deionized water (DI only control) and hydrous ferric oxide (HFO only control) with no sodium sulfide added to them.

CHC stock solution was prepared in a 160 mL serum bottle containing Milli-Q water by injecting 20 μL of pure phase CHCs. 25-100 μL of select CHCs were injected into sealed experimental and control reactors and then were placed on an end-over-end rotary shaker at 45 rpm. 50 μL of the headspace were periodically extracted using a gas tight syringe (Hamilton, Reno, NV) and injected into a gas chromatograph to quantify the CHCs and their degradation products. The reactors were homogenously mixed on the rotary shaker for the entire duration of the experiment except during sample extraction.

1.2.3 Analytical Methods

CHCs and degradation products were analyzed in a gas chromatograph (7890 GC system; Agilent Technologies) equipped with electron capture detector (ECD) and flame ionization detector (FID). CHCs were separated on HP 624 (30 m x 0.32 mm x 0.25 μm; Agilent Technologies) capillary column and were visible on ECD. Non-chlorinated hydrocarbons were separated on Gas Pro capillary column (30 m x 0.32 mm x 0.25 μm, Agilent Technologies) and were visible on FID. Helium was used as a carrier gas at a constant flow of 2.5 mL min^{-1}. The GC method was split/splitless inlet = 250 °C, oven temperature = 100 °C (isothermal). Nitrogen gas (N_2) was used as the makeup gas with flow rate of 25 mL min^{-1} for ECD. The flow rate for H_2 and air was 450 and 30 mL min^{-1} respectively for FID.

1.2.4 Data Treatment

The peak area values obtained from GC-ECD/FID was converted to chemical amounts (micromoles) using slope of the calibration curve. The values reported in amount-time charts are averages of triplicate reactors, and the standard deviations are

shown as error bars in the charts. The apparent lack of error bars in the figures indicates that the error bars are very small and are hidden behind the size of the data point symbol.

The average amount of the chemical obtained vs. time was plotted in MS Excel and a pseudo first-order rate model was fitted to the amount-time data set; the value of the exponent of the fitted exponential decay equation provides the observed rate constant of degradation (k_{obs}). The data plots often showed a faster initial kinetics, followed by slower kinetics; on this basis, the degradation curves were divided into two phases, and the rate constants were estimated for an initial fast phase (k_{obs1}) and a slower second phase (k_{obs2}).

The observed rate constant (k_{obs}) values were divided by HFO concentration (g/L) in the reactor in order to estimate the mass normalized rate constant (k_M) of CHC degradation. Published values of surface area normalized rate constant (k_{SA}) were converted to mass normalized (k_M) for comparison. Though, transformation reactions are supposed to occur on mineral surface and reaction kinetics is expected to be proportional to its specific surface area of the mineral (He et al., 2015), it is difficult to get accurate surface area by BET method as HFO particles can aggregate upon drying. BET measurements of the HFO surface area upon drying may not be representative of real surface area, and currently, there are no analytical methods that can measure the surface area of nanoparticles in suspension accurately (Kumar et al., 2018).

The carbon mass balance for each experiment is also presented, which includes the sum of mole fraction of the reactant and all products obtained for each sampling. Data

from the DI and HFO control reactors are also included in the charts but they are not discussed unless there is a significant loss in those reactors over the experimental period.

1.3 RESULTS AND DISCUSSIONS

1.3.1 Degradation of Carbon Tetrachloride with Sulfide-Treated HFO

CT degradation with 1.4 g/L sulfide-treated HFO was faster (k_{obs1}= $4.0*10^{-2}$ hr^{-1}; k_{m1}=$2.9*10^{-2}$ L g^{-1} hr^{-1}) in first six hours with CF as the only observed degradation product (Figure 1A). The reaction slowed afterwards (k_{obs2}= $2.2*10^{-2}$; k_{m2}=$1.6*10^{-2}$ L g^{-1} hr^{-1}) (Figure 1A). After ~73 hours, remaining CT mole fraction was 0.20 and CF mole fraction yield was 0.05 with mass balance of 0.25 (Figure 1B). By ~73 hours, HFO control did not show any loss, while DI control showed a loss of 16% (Figure 1A). A high-resolution study was conducted for the first six hours to observe transient species, but none were seen except chloroform (Figure 1C).

Hanoch et al. (2006) studied the reactivity of following sulfide-treated iron oxides towards CT: goethite (k_m=$1.2*10^{-3}$ L g^{-1} hr^{-1}), hematite (k_m=$1.9*10^{-4}$ L g^{-1} hr^{-1}), and magnetite (k_m=$4.3*10^{-4}$ L g^{-1} hr^{-1}), where the reported values are a magnitude lower than k_m observed in this study with sulfide treated HFO. Butler and Hayes (2000) observed k_m = $6.4*10^{-3}$ L g^{-1} hr^{-1} for CT degradation with FeS precipitated by reaction of Fe(II) and HS$^-$ (normalized to FeS formed). The higher kinetics observed with sulfide-treated HFO observed in the present study may be attributed to the higher specific surface area of the starting phase.

11

The production of a small amount of chloroform (~5%) and the absence of other reduction daughter products, such as dichloromethane (DCM) and methane, suggests that hydrogenolysis is perhaps not a major degradation pathway for CT. Hanoch et al. (2006) also did not observe significant CF production (~1%) with sulfide-treated iron oxides. However, with lab-precipitated FeS, higher CF yield (46%) has been observed for CT degradation (Buttler and Hayes, 2000) but it remains unclear why lab-precipitated FeS showed higher CF yield. Suppression of hydrogenolytic pathway has also been observed with sulfide-treated vermiculite and biotite by Kriegman-King and Reinhard (1992); they observed 10-15 mole% CF production, and the rest (80-85%) of CCl_4 was transformed to CO_2 via CS_2. Likewise, CS_2 has also been detected during CT degradation with commercial FeS obtained from Aldrich (Kenneke and Weber, 2003).

One possible pathway for formation of CS_2 is via nucleophilic substitution reaction of CT with bisulfide or other intermediate sulfur species: polysulfide and bisulfite species (Kriegman-King and Reinhard 1992). The low mass balance during CT degradation may be due to production of CS_2 which was not detectable by our analytical method.

As such, without the major degradation product being quantified, it is difficult to conclude the major mechanism and the species responsible for it. Future work should explore possibilities for other by-products such as CS_2, and CO_2.

1.3.2 Degradation of Chloroform with Sulfide-Treated HFO

The degradation of chloroform (CF) with 1.4 g/L sulfide-treated HFO was very slow ($k_{obs}= 1.7*10^{-5}$ hr^{-1}; $k_m = 1.2*10^{-5}$ L g^{-1} hr^{-1}) over the course of over 71 days (Figure

1.2A). However, the R^2 of the pseudo first order fit is poor as well the readings on controls seem to increase towards the end. DI shows an increase of 17% in the reading whereas HFO shows an increase of reading by 24% (Figure 2B). Reduction products such as DCM and methane were not observed. Kenneke and Weber (2003) observed much faster reaction ~ 43 times ($k_{obs} = 4.6*10^{-4}$ L g^{-1} hr^{-1}) with technical grade FeS obtained from Aldrich (Experimental Conditions: 44 g/L, pH 7.8). However, they observed zero valent iron in the x-ray analysis of FeS, which might be the reason behind higher reactivity. In their work, reduction products were not seen.

1.3.3 Degradation of 1,1,2-Trichloroethane with Sulfide-Treated HFO

1,1,2-TCA degradation with 1.4 g/L sulfide-treated HFO was modest ($k_{obs1} =$ 2.5*10^{-1} hr^{-1}; $k_{m1} = 1.8*10^{-1}$ L g^{-1} hr^{-1}) in first six hours with 1,1-DCE as the only observed degradation byproduct (Figure 1.3A), but the reaction kinetics slowed afterwards ($k_{obs2} = 2.0*10^{-1}$ hr^{-1}; $k_{m2} = 1.4*10^{-1}$ L g^{-1} hr^{-1}; Figure 1.3A). At ~25 hours, the remaining mole fraction of 1,1,2-TCA was 0.01, and 1,1-DCE mole fraction yield was 0.33 making the carbon mass balance = 0.34 (Figure 1.3B). By ~25 hours, the HFO control reactor showed a loss of 7% while DI control reactor did not show any loss (Figure 1.3A). A high-resolution study conducted for first seven hours did not reveal any transient species (Figure 1.3C).

The production of 1,1-DCE from 1,1,2-TCA degradation is via dehydrohalogenation pathway. This finding is somewhat different than Butler and Hayes (2000) in which the authors observed 22% degradation over a course of 120 days with 1,1-DCE (7%) and VC (1%) with 10 g/L FeS at pH 8.3. Their aqueous medium control

reactor (without FeS) showed 7% conversion of 1,1,2-TCA to 1,1-DCE, which suggests very little net reactivity of the precipitated FeS phase towards 1,1,2-TCA. The results also show that the sulfide-treated HFO in this study expresses a greater reactivity towards 1,1,2-TCA in comparison to precipitated FeS.

1.3.4 Degradation of 1,1,1,2-Tetrachloroethane with Sulfide-Treated HFO

The degradation of 1,1,1,2- Tetrachloroethane (1,1,1,2-TeCA) with 1.4 g/L sulfide-treated HFO was faster (k_{obs1} = 8*10^{-2} hr^{-1}; k_{m1} = 6*10^{-2} L g^{-1} hr^{-1}) in first six-hours with TCE as a major reaction byproduct, and 1,1-DCE as a minor product (Figure 1.4A). The reaction slowed afterwards (k_{obs1} = 3*10^{-2} hr^{-1}; k_{m1} = 2*10^{-2} L g^{-1} hr^{-1}) (Figure 1.4A). Over a longer-term (at ~144 hours), the remaining 1,1,1,2-TeCA mole fraction was 0.02, where TCE and 1,1-DCE mole fraction yields were 0.29 and 0.04 (Figure 1.4B). The carbon mass balance at ~144 hours was ~0.35 (Figure 1.4B). In the same period, the DI control and HFO control reactors showed losses of 21 and 7%, respectively (Figure 1.4B). This indicates that dehydrohalogenation (TCE formation) may be the major pathway for 1,1,1,2-TeCA transformation with sulfide-treated HFO, whereas β elimination (1,1-DCE formation) is a minor pathway. None of the potential products of 1,1,1,2-TeCA degradation via hydrogenolysis pathway (i.e., 1,1,2-TCA, 1,1-DCA and 1,2-DCA) was observed during the experiment.

Butler and Hayes (2000) observed a slower kinetics and somewhat different pathway of 1,1,1,2-TeCA reaction with lab-precipitated FeS (10 g/L FeS at pH 8.3), showing k_{obs} = 3*10^{-2} hr^{-1}; k_m = 3*10^{-3} L g^{-1} hr^{-1}, with 62% conversion to 1,1-DCE but no

TCE thus suggesting β elimination to be the degradation pathway. This may be attributed to the differences in the reactivity of lab-precipitated FeS and sulfide-treated HFO.

1.3.5 Degradation of 1,1,2,2-Tetrachloroethane with Sulfide-Treated HFO

1,1,2,2- Tetrachloroethane (1,1,1,2-TeCA) degradation with 1.4 g/L sulfide-treated HFO was the fastest among observed kinetics for the other CHCs in this study. At first sampling ~3.5 hours, all of 1,1,2,2-TeCA was removed from the reactors (Figure 1.5A), where TCE was the only observed degradation product with a mole fraction yield of ~1.00 and a carbon mass balance ~1.00 (Figure 1.5B). By ~50 hours, both DI and HFO control reactors did not show any loss (Figure 1.5A). A high-resolution sampling with increased concentration (~10 times in Figure 1.5A) of 1,1,2,2-TeCA also showed a complete conversion to TCE by the first sampling in 1 hour (Figure 1.5B).

The observed abiotic transformation of 1,1,2,2-TeCA to TCE likely occurred by dehydrohalogenation. This finding is in contrast with a study with 10 g/L lab-precipitated FeS at pH 8.3 (Butler and Hayes, 2000) who reported a much slower degradation kinetics ($k_{obs} = 3.05*10^{-2}$ hr^{-1}; $k_m = 3.05*10^{-3}$ Lg^{-1} hr^{-1}) and differences in byproduct distribution with 1,1,2,2-TeCA degrading to TCE (58%), acetylene (~14%) and minor amount of *trans*-DCE and *cis*-DCE. However, the aqueous medium control reactor (without FeS) of Butler and Hayes (2000) showed significant transformation of 1,1,2,2-TeCA to TCE, which they attributed to species such as hydroxide ion. However, no significant transformation of 1,1,2,2, -TeCA to TCE was observed in this work with DI or HFO controls.

1.3.6 Degradation of Trichloroethene with Sulfide-Treated HFO

Trichloroethene (TCE) degradation with 1.4 g/L of sulfide-treated HFO was examined at three initial pHs: 7, 8 and 9 for ~ 80 days. At all these pHs, the loss of TCE in the reactors containing the sulfide-treated HFO were observed to be almost equal to the TCE loss in the DI control reactors (Figures 1.6A, 1.6 B, 1.7A and 1.7 C): pH 7 (reactors ~11%, and DI control ~ 14%), pH 8 (reactors ~17 % and DI control ~ 19%) and pH 10 (reactors ~ 23 % and DI control ~ 23%). Such observed loss may have been due to adsorption to glass container and the stopper, loss of volatile phase during sampling, etc. As such, no significant degradation of TCE was observed with sulfide-treated HFO under the experimental conditions. However, TCE degradation with iron sulfide through dihaloelimination pathway to acetylene with 10 g/L lab-precipitated FeS at pH 7.3 has been reported previously (Butler and Hayes, 2001). Likewise, He et al., (2010) also observed TCE degradation with 20 g/L FeS through dihaloelimination pathway to acetylene. Chlorinated ethenes such as TCE may not undergo dehydrohalogenation reaction, which is consistent with our observation (Cwiertny and Scherer, 2010b).

1.3.7 CHC Degradation Pathways

Based on the reaction byproducts observed in this study, chlorinated ethanes degraded with sulfide-treated HFO (Table 1.1) via dehydrohalogenation pathway. Although, it remains unclear which chemical species is responsible for this mechanism, the observed pattern of reactivity: 1,1,2,2-TeCA > 1,1,2-TCA (product 1,1-DCE) > 1,1,1,2-TeCA is in good agreement with Walraevens et al., (1974) who studied dehydrohalogenation induced by OH$^-$ ions. No removal of chlorinated ethenes also

supports dehydrohalogenation may be the major mechanism in the system. The small amount of CF (~5%) produced from CT degradation, and 1,1-DCE (~5%) produced from 1,1,1,2-TeCA degradation shows that reductive hydrogenolysis and β elimination pathways, respectively, is a minor pathway unlike what is seen with lab-precipitated FeS.

1.4 CONCLUSIONS

- CT, 1,1,2-TeCA, 1,1,1,2-TeCA and 1,1,2,2-TeCA showed faster degradation kinetics with sulfide-treated HFO, whereas CF and TCE did not show appreciable degradation.

- Reaction byproducts included 1,1-DCE from 1,1,2-TCA, TCE from 1,1,1,2-TeCA and 1,1,2,2-TeCA, which suggests that dehydrohalogenation is a major pathway for degradation, and reduction (CF formation from CT via hydrogenolysis, and 1,1-DCE from 1,1,1,2-TeCA via β elimination) may be minor pathways under the experimental conditions of this study.

- The pathways of CHC degradation by sulfide-treated HFO vs. lab-precipitated FeS show significant differences. Under the experimental conditions of this study, dehydrohalogenation is the major pathway of CHC degradation, whereas reductive pathway has been demonstrated with lab-precipitated phase FeS, which suggested differences in the underlying reaction mechanisms.

REFERENCES

Amir, A. and Lee, W. (2012). Enhanced reductive dechlorination of tetrachloroethene during reduction of cobalamin (III) by nano-mackinawite. *Journal of Hazardous Materials, 235,* 359-366.

Butler, E. C. and Hayes, K. F. (1998). Effects of solution composition and pH on the reductive dechlorination of hexachloroethane by iron sulfide. *Environmental Science & Technology, 32*(9), 1276-1284.

Butler, E. C. and Hayes, K. F. (1999). Kinetics of the transformation of trichloroethylene and tetrachloroethylene by iron sulfide. *Environmental Science & Technology, 33*(12), 2021-2027.

Butler, E.C. and Hayes, K.F. (2000). Kinetics of the transformation of halogenated aliphatic compounds by iron sulfide. *Environmental Science & Technology, 34*, 422-429.

Butler, E. C. and Hayes, K. F. (2001). Factors influencing rates and products in the transformation of trichloroethylene by iron sulfide and iron metal. *Environmental Science & Technology, 35*(19), 3884-3891.

Cwiertny, D.M. and Scherer, M.M. (2010a). Chlorinated solvent chemistry: Structures, nomenclature and properties. In *In Situ Remediation of Chlorinated Solvent Plumes (*pp. 29-37). Springer, New York, NY.

Cwiertny, D.M. and Scherer, M.M. (2010b). Abiotic Processes affecting the remediation of chlorinated solvents. In *In Situ Remediation of Chlorinated Solvent Plumes* (pp. 69-108). Springer, New York, NY.

Cornell, R. M. and Schwertmann, U. (1996). The iron oxides: structure, properties, reactions, occurrences and uses. Wiley-VCH.

Christensen, T.H., Bjerg, P.L., Banwart, S.A., Jakobsen, R., Heron, G. and Albrechtsen, H.J. (2000). Characterization of redox conditions in groundwater contaminant plumes. *Journal of Contaminant Hydrology, 45,* 165-241.

Davis, A., Fennemore, G.G., Peck, C., Walker, C.R., McIlwraith, J. and Thomas, S. (2003). Degradation of carbon tetrachloride in a reducing groundwater environment: Implications for natural attenuation. *Applied Geochemistry, 18,* 503-525.

He, Y. T., Wilson, J. T. and Wilkin, R. T. (2010). Impact of iron sulfide transformation on trichloroethylene degradation. *Geochimica et Cosmochimica Acta, 74*(7), 2025-2039

He, Y.T., Wilson, J.T., Su, C. and Wilkin, R.T. (2015). Review of abiotic degradation of chlorinated solvents by reactive iron minerals in aquifers. *Groundwater Monitoring & Remediation, 35(3)*, pp.57-75.

Hanoch, R., Shao, H. and Butler, E.C. (2006). Transformation of carbon tetrachloride by bisulfide treated goethite, hematite, magnetite, and kaolinite. *Chemosphere 63,* 323-334.

Huang, B. B., Lei, C., Wei, C. H. and Zeng, G. M. (2014). Chlorinated volatile organic compounds (Cl-VOCs) in environment - sources, potential human health impacts, and current remediation technologies. *Environment International, 71,* 118-138.

He, Y.T., Wilson, J.T. and Wilkin, R.T. (2010). Impact of iron sulfide transformation on trichloroethylene degradation. *Geochimica Et Cosmochimica Acta 74,* 2025-2039.

Jeong, H. Y. and Hayes, K. F. (2007). Reductive dechlorination of tetrachloroethylene and trichloroethylene by mackinawite (FeS) in the presence of metals: Reaction rates. *Environmental Science & Technology, 41*(18), 6390-6396.

Kenneke, J.F. and Weber, E.J. (2003). Reductive dehalogenation of halomethanes in iron- and sulfate-reducing sediments. 1. Reactivity pattern analysis. *Environmental Science & Technology 37,* 713-720.

Kriegman-King, M.R. and Reinhard, M. (1992). Transformation of carbon tetrachloride in the presence of sulfide, biotite, and vermiculite. *Environmental Science & Technology, 26(11)*, 2198-2206.

Kumar, N., Pacheco, J. L., Noël, V., Dublet, G., and Brown, G. E. (2018). Sulfidation mechanisms of Fe(iii)-(oxyhydr)oxide nanoparticles: A spectroscopic study. *Environmental Science: Nano, 5(4)*, 1012-1026.

Maithreepala, R. A. and Doong, R. A. (2005). Enhanced dechlorination of chlorinated methanes and ethenes by chloride green rust in the presence of copper (II). *Environmental Science and Technology*, *39*(11), 4082-4090.

McCormick, M. L., Bouwer, E. J. and Adriaens, P. (2002). Carbon tetrachloride transformation in a model iron-reducing culture: relative kinetics of biotic and abiotic reactions. *Environmental Science & Technology*, *36*(3), 403-410.

Miao, Z., Brusseau, M.L., Carroll, K.C., Carreon-Diazconti, C. and Johnson, B. (2012). Sulfate reduction in groundwater: characterization and applications for remediation. *Environmental Geochemistry and Health, 34,* 539-550.

Moran, M. J., Zogorski, J. S. and Squillace, P. J. (2007). Chlorinated solvents in groundwater of the United States. *Environmental Science & Technology, 41*(1), 74-81.

O'Loughlin, E. J., Kemner, K. M. and Burris, D. R. (2003). Effects of Ag[I], Au[III], and Cu[II] on the reductive dechlorination of carbon tetrachloride by green rust. *Environmental Science & Technology*, *37*(13), 2905-2912.

Pankow, J. F. and Cherry, J. A. (1996). Dense chlorinated solvents in groundwater; background and history of the problem. In (pp. 1-52). United States: Waterloo Press: Portland, OR, United States.

Pyzik, A. J. and Sommer, S. E. (1981). Sedimentary iron monosulfides - kinetics and mechanism of formation. *Geochimica et Cosmochimica Acta, 45*(5), 687-698.

Rickard, D. and Luther, G. W. (2007). Chemistry of iron sulfides. *Chemical Reviews, 107(2)*, 514-562.

United States Environmental Protection Agency. (2017). Superfund Public User Database public information version: 2.00 list-010 top 20 contaminants at superfund sites https://semspub.epa.gov/work/HQ/196735.pdf (accessed 8.17.2017)

Villacis-Garcia, M., Ugalde-Arzate, M., Vaca-Escobar, K., Villalobos, M., Zanella, R. and Martinez-Villegas, N. (2015). Laboratory synthesis of goethite and ferrihydrite of controlled particle sizes. *Boletin De La Sociedad Geologica Mexicana, 67,* 433-446.

Villalobos, M. and Antelo, J. (2011). A unified surface structural model for ferrihydrite: Proton charge, electrolyte binding, and arsenate adsorption. *Revista Internacional De Contaminacion Ambiental, 27,* 139-151.

Walraevens, R., Trouillet, P. and Devos, A. (1974). Basic elimination of HCl from chlorinated ethanes. *International Journal of Chemical Kinetics*, *6(6)*, 777-786.

Wong, M. S., Alvarez, P. J. J., Fang, Y. L., Akcin, N., Nutt, M. O., Miller, J. T., et al. (2009). Cleaner water using bimetallic nanoparticle catalysts. *Journal of Chemical Technology and Biotechnology, 84*(2), 158-166.

Wiedemeier, T.H., Wilson, J.T., Hansen, J.E., Chapelle, F.H. and Swanson, M.A. (1996). Technical Protocol for Evaluating Natural Attenuation of Chlorinated Solvents in Groundwater. Revision 1. Air Force Center for Environmental Excellence Brooks AFB, Texas.

Zachara, J. M., Fredrickson, J. K., Li, S. M., Kennedy, D. W., Smith, S. C. and Gassman, P. L. (1998). Bacterial reduction of crystalline Fe^{3+} oxides in single phase suspensions and subsurface materials. *American Mineralogist, 83(11)*, 1426-1443.

Zhang, M., He, F., Zhao, D. Y. and Hao, X. D. (2011). Degradation of soil-sorbed trichloroethylene by stabilized zero valent iron nanoparticles: Effects of sorption, surfactants, and natural organic matter. *Water Research, 45*(7), 2401-2414.
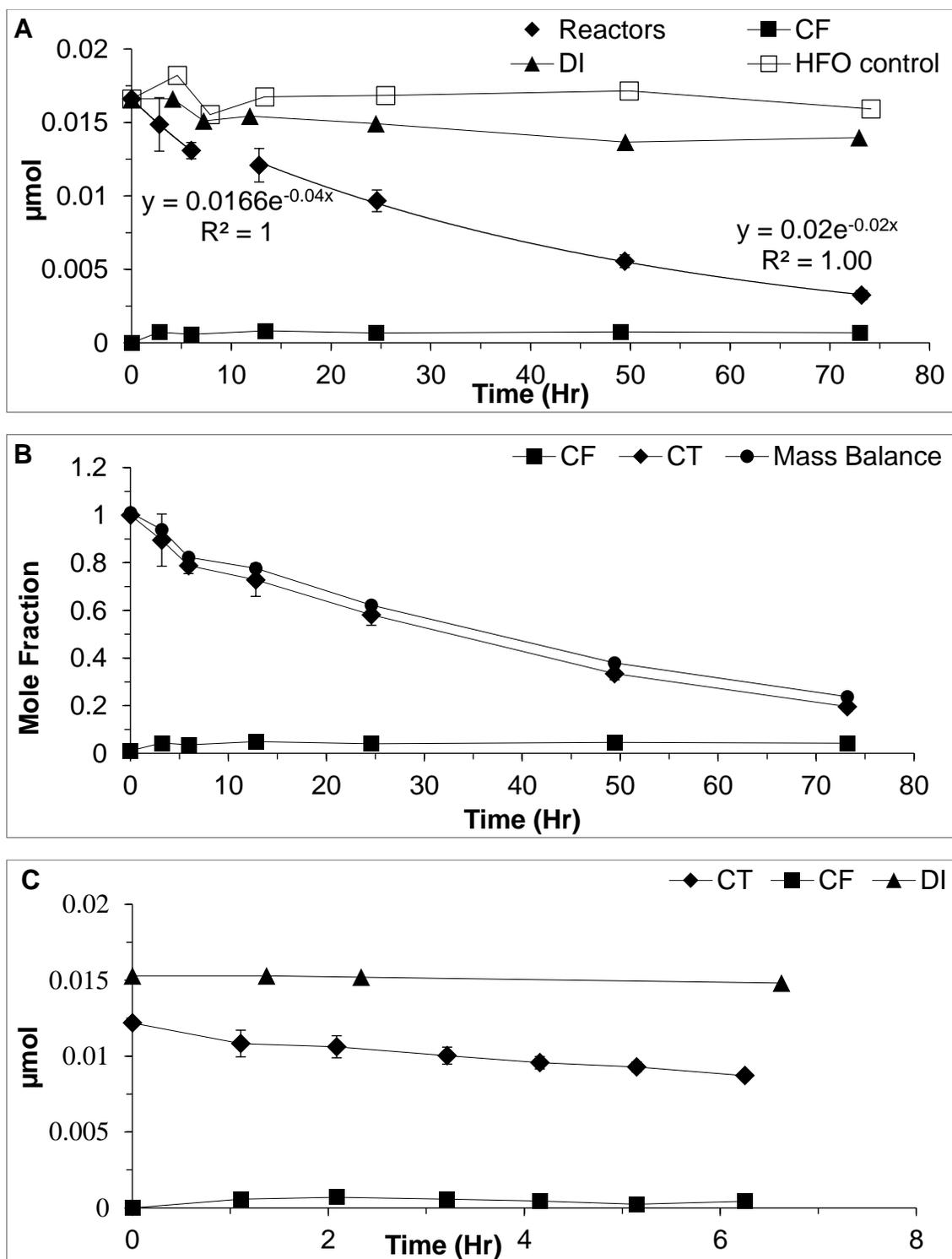
Figure 1.1: CT degradation with 1.4 g/L sulfide-treated HFO at pH 7 (TAPSO buffer: 37.5 mM); Fe: HS⁻ ratio = 1:1.5 (i.e., 25 mM HFO:37.5 mM Na₂S). (A) Long term degradation, product distribution and controls, (B) Mass balance and (C) Short term degradation

22
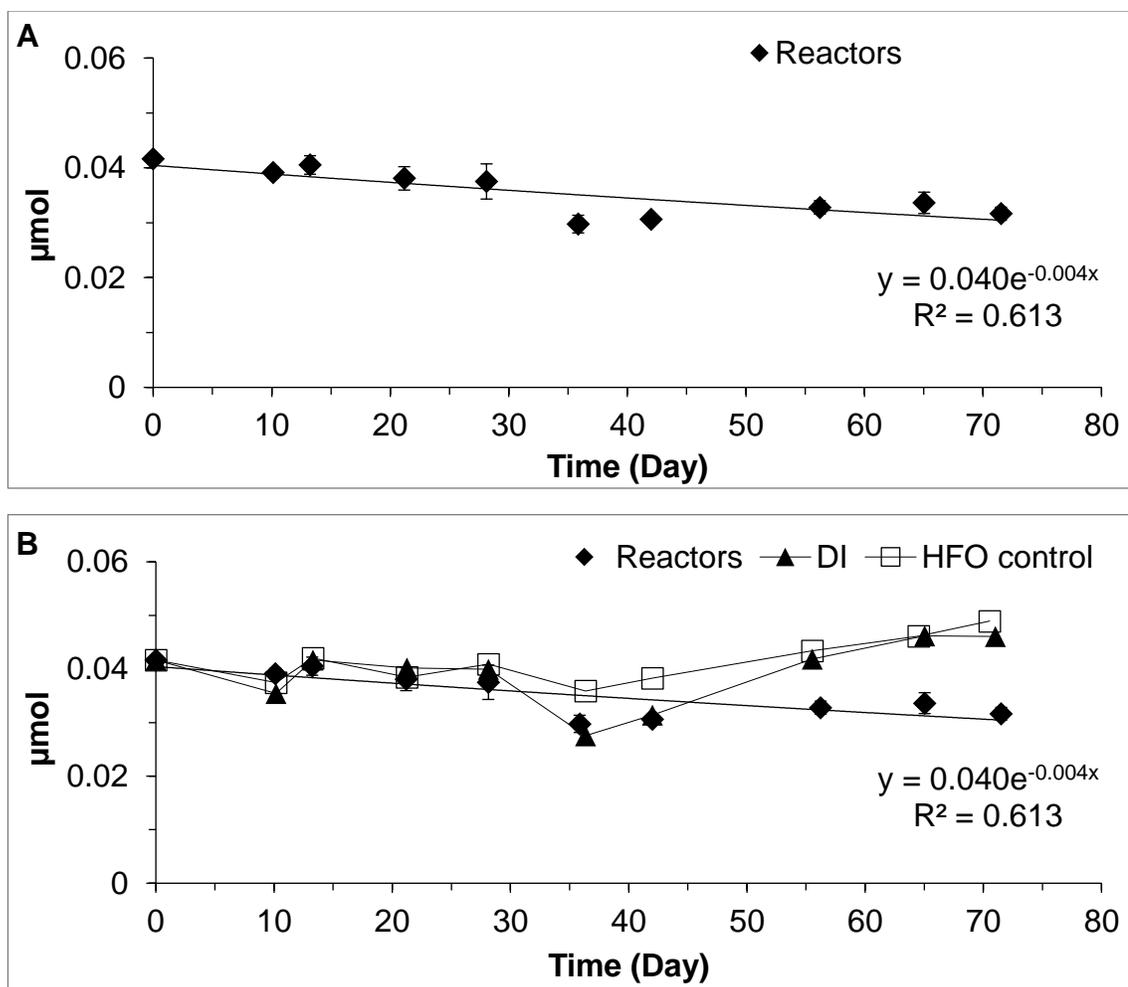
Figure 1.2: CF degradation with 1.4 g/L sulfide-treated HFO at pH 7 (TAPSO buffer: 37.5 mM); Fe: HS⁻ ratio = 1:1.5 (i.e., 25 mM HFO:37.5 mM Na$_2$S). (A) Degradation curve with exponential fit and (B) Comparison with DI and HFO control
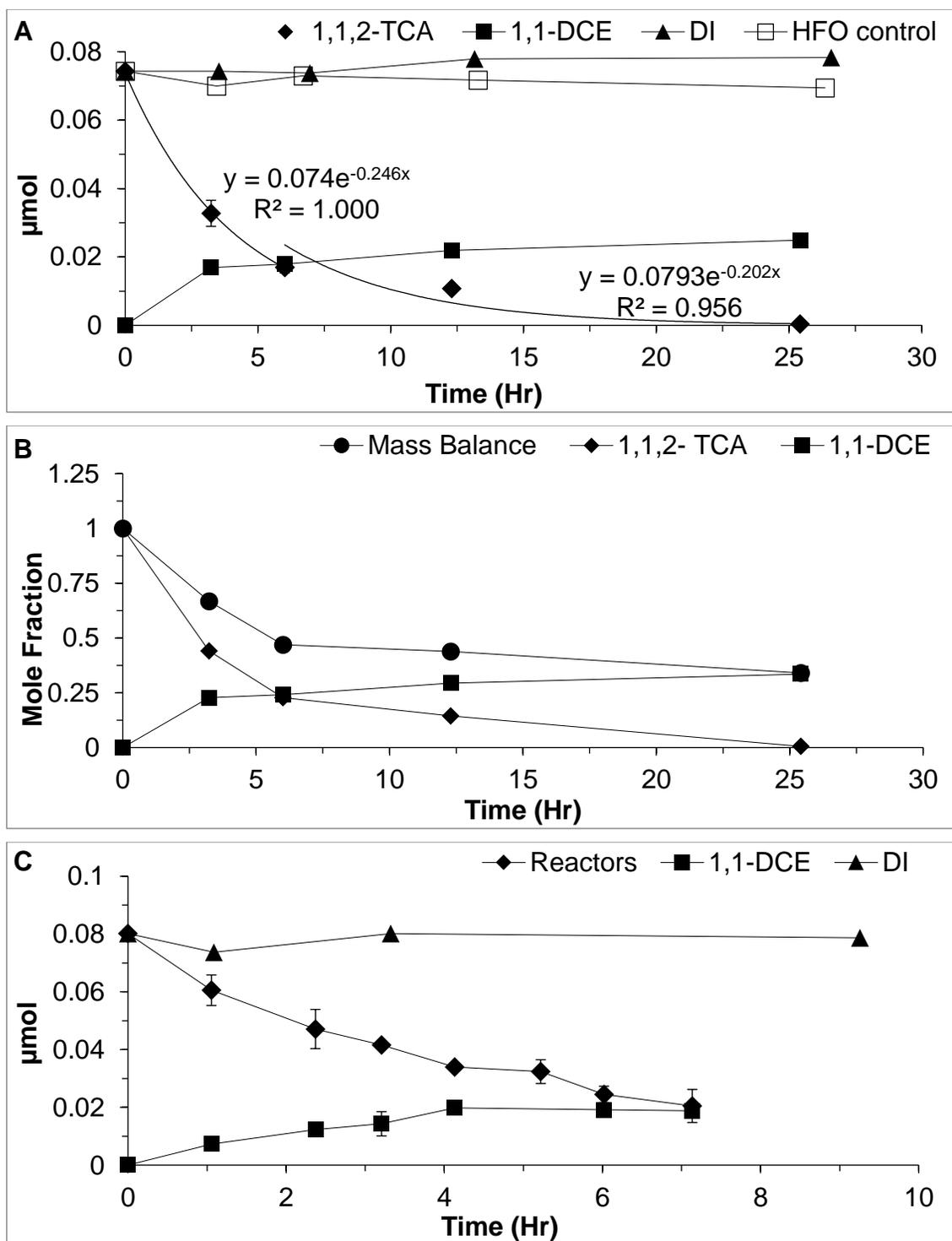
Figure 1.3: 1,1,2-TCA degradation with 1.4 g/L sulfide-treated HFO at pH 7 (TAPSO buffer: 37.5 mM); Fe: HS⁻ ratio =1:1.5 (i.e.,25 mM HFO:37.5 mM Na₂S). (A)Long-term degradation, product distribution, and controls, (B) Mass Balance and (C) Short term degradation.
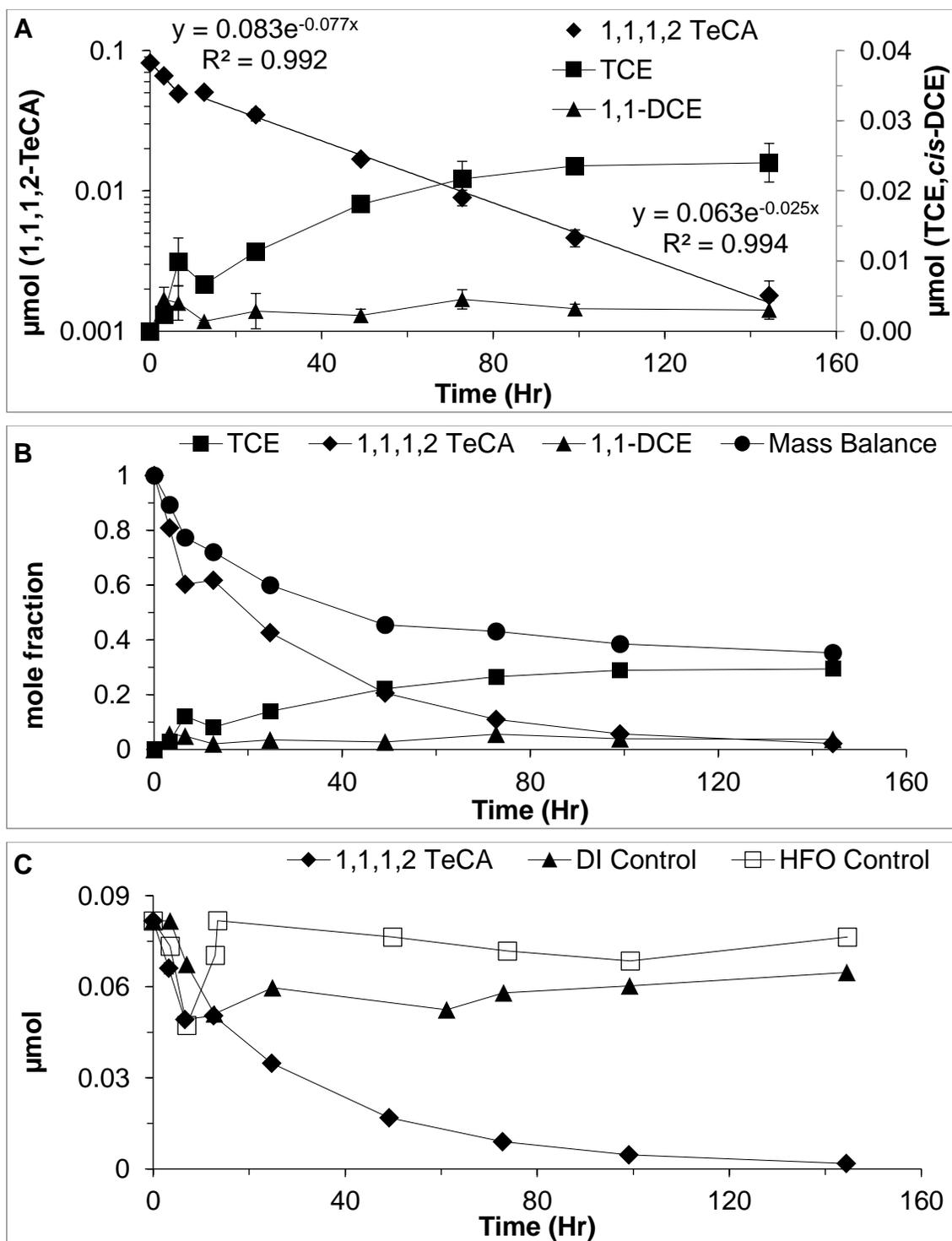
Figure 1.4: 1,1,1, 2-TCA degradation with 1.4 g/L sulfide-treated HFO at pH 7 HFO
(TAPSO buffer: 37.5 mM); Fe: HS^- ratio =1:1.5 (i.e., 25 mM HFO:37.5 mM Na_2S). (A)
Biphasic rate constants with products, (B) Mass balance with products, and (C)
Comparison with controls
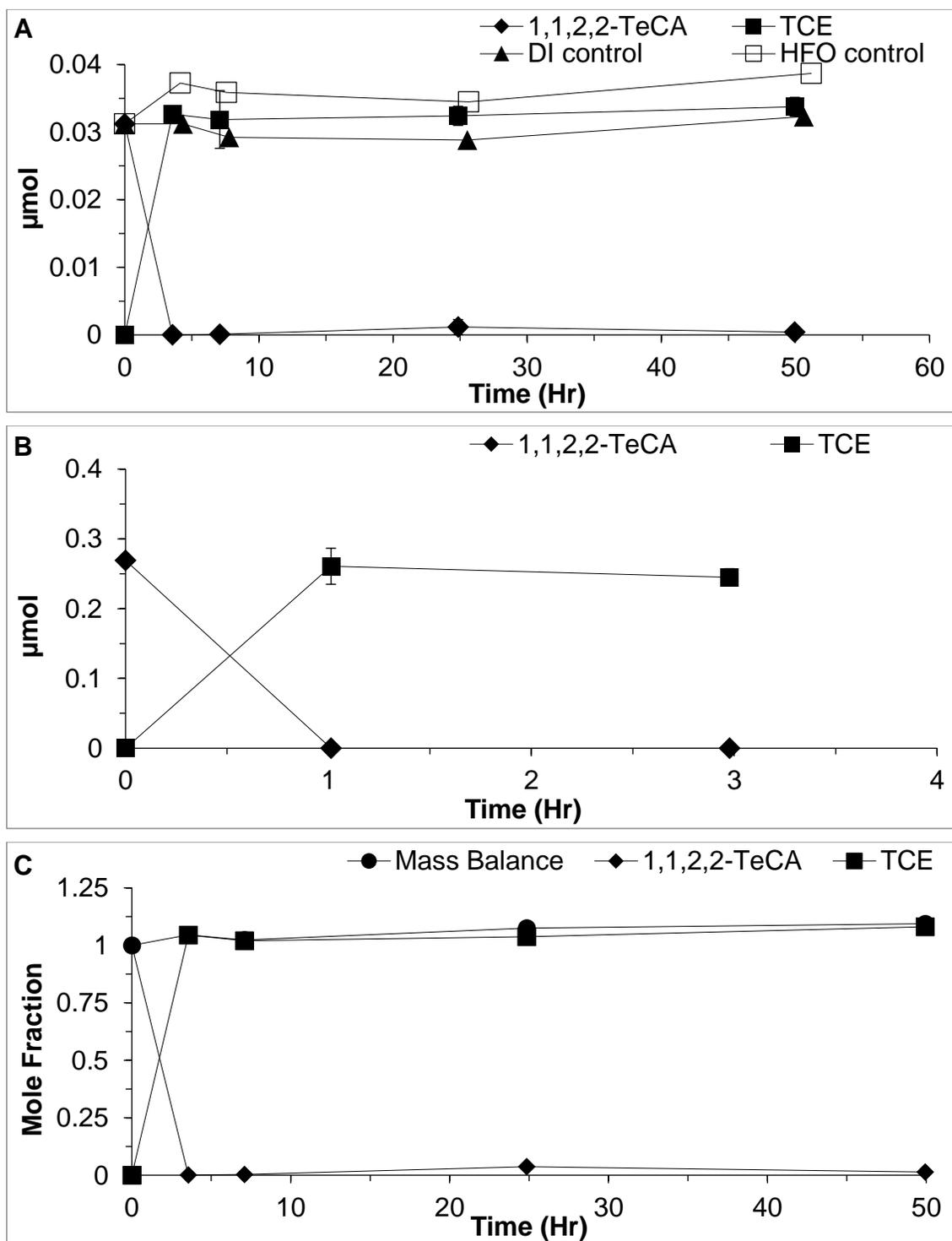
Figure 1.5: 1,1,2,2-TeCA degradation with 1.4 g/L sulfide-treated HFO at pH 7 HFO (TAPSO buffer: 37.5 mM); Fe: HS⁻ ratio =1:1.5 (i.e., 25 mM HFO:37.5 mM Na$_2$S). (A) Degradation curve, product distribution and comparison with DI and HFO controls, (B) High resolution sampling with higher concentration and (C) Mass Balance
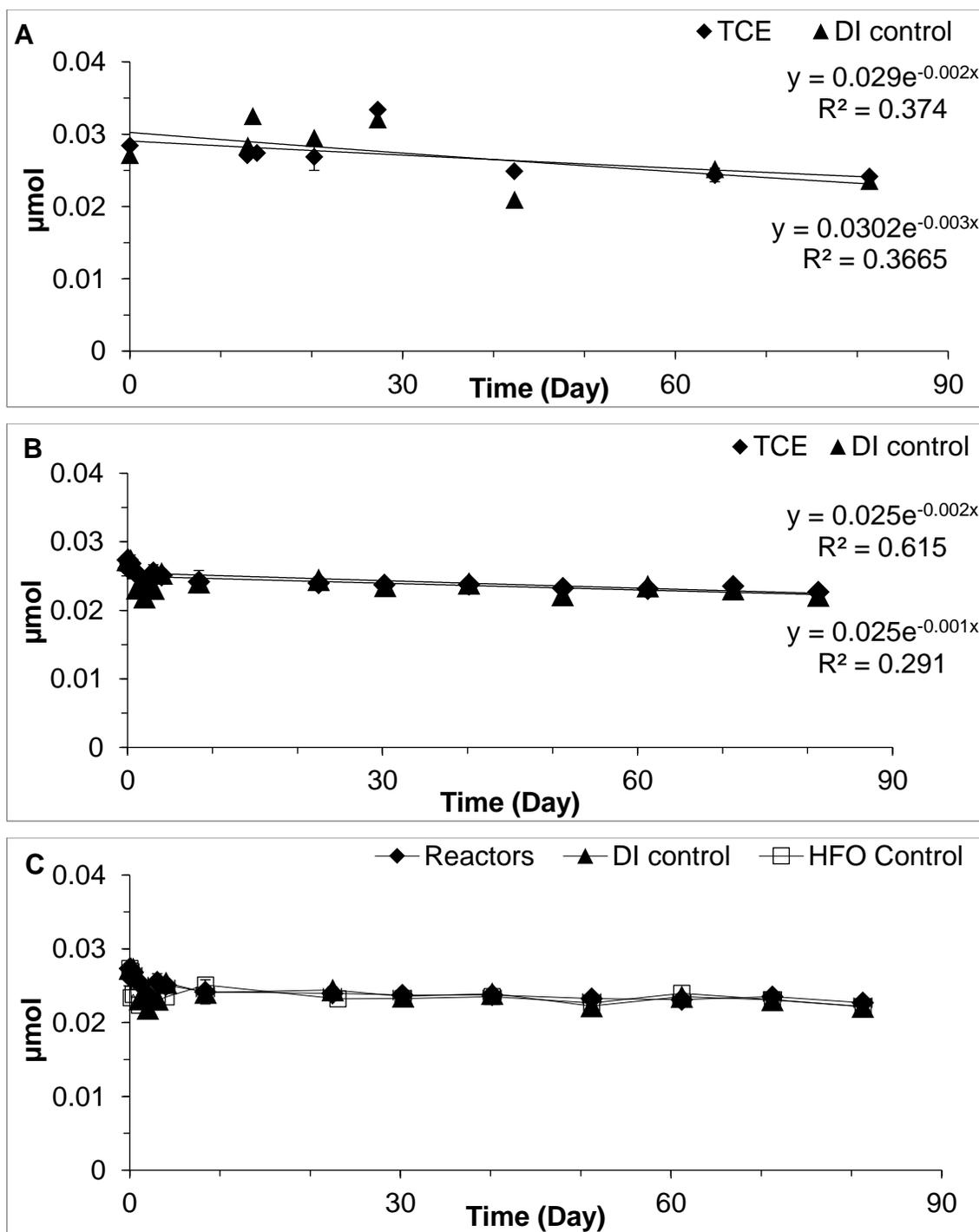
Figure 1.6: (A) TCE degradation with 1.4 g/L sulfide- treated HFO at pH 7 (TAPSO: 37.5 mM); Fe: HS^- ratio =1:1.5 (i.e., 25 mM HFO:37.5 mM Na_2S). HFO control was not employed for this experiment. (B) TCE degradation with 1.4 g/L sulfide- treated HFO at pH 8 (TAPSO: 37.5 mM); Fe: HS^- ratio=1:1.5 (i.e., 25 mM HFO:37.5 mM Na_2S), and (C) Comparison with HFO and DI control for pH 8 experiment (Note: The exponential equation on top is for reactors and on bottom is for DI controls)
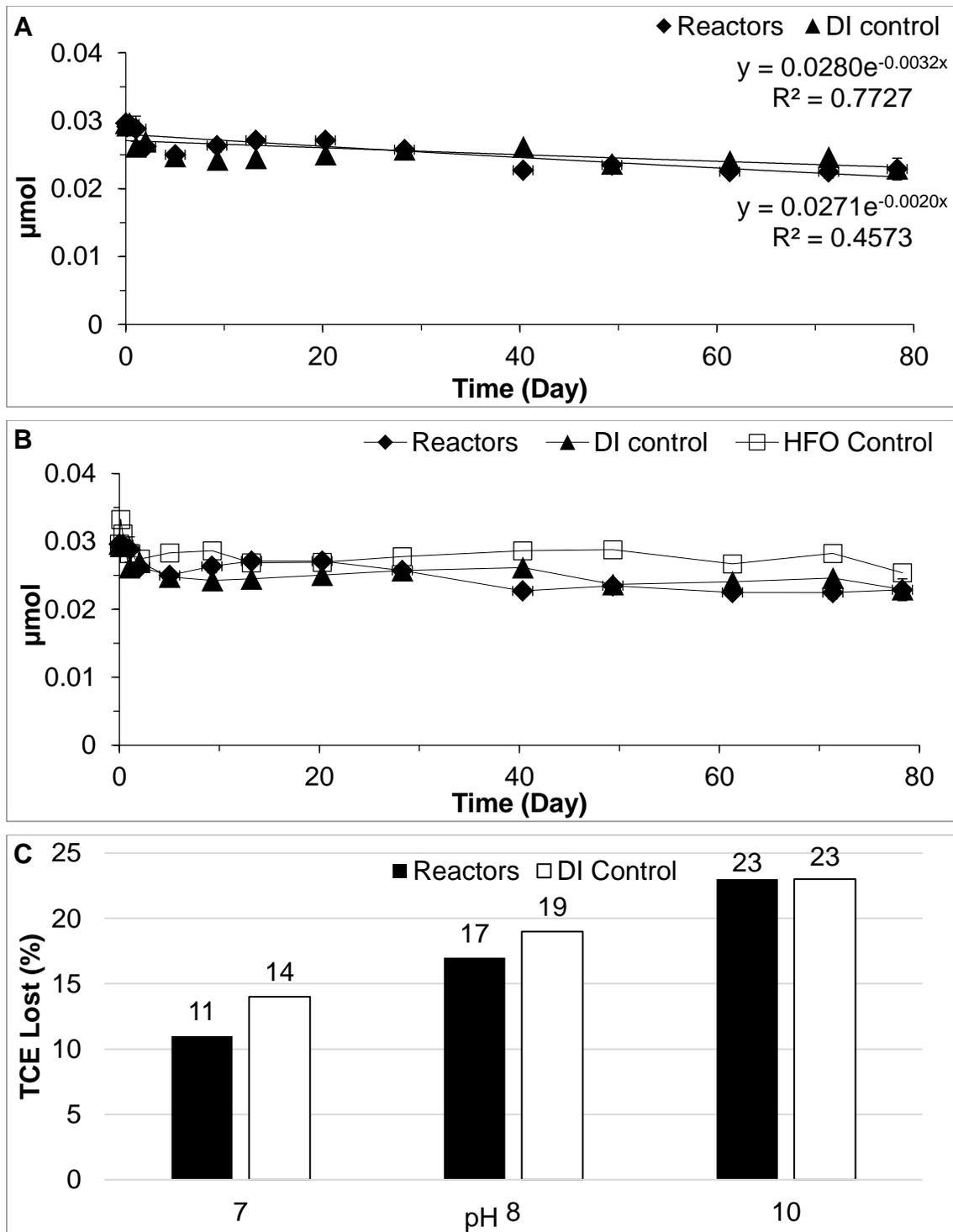
Figure 1.7: TCE degradation with 1.4 g/L sulfide- treated HFO at pH 10 with 1.4 g/L sulfide- treated HFO at pH 7 (TAPSO buffer: 37.5 mM); Fe: HS^- ratio =1:1.5 (i.e., 25 mM HFO:37.5 mM Na_2S). (A) pseudo first order fit for reactors and DI, and (B) Comparison with HFO and DI controls (C) TCE lost (%) in reactors and control

Table 1.1: Degradation of select CHCs with 1.4 g/L sulfide-treated HFO. Shows initial CHC amount, initial pH, pseudo first-order degradation rate constants (initial k_{obs1}, and long-term k_{obs2}) along with reaction products and degradation pathway(s)

			Fast Reactions					
CHC	Initial amount (μmol)	pH	k_{obs1}		k_{obs2}		Byproducts	Degradation Pathway
			$Lg^{-1} hr^{-1}$	R^2	$Lg^{-1} hr^{-1}$	R^2		
CT	0.0166	7	0.029	1.00	0.016	0.99	CF (4%)	Hydrogenolysis
1,1,2-TCA	0.0743	7	0.202	1.00	0.179	1.00	1,1-DCE (33%)	Dehydrohalogenation
1,1,1,2-TeCA	0.0817	7	0.057	0.99	0.021	0.99	TCE (29%) 1,1-DCE (4%)	Dehydrohalogenation, B-elimination
1,1,2,2-TeCA	0.03123	7	*				TCE (100%)	Dehydrohalogenation

(* too fast to be quantified)

Table 1.2: Degradation of Select CHCs with 1.4 g/L sulfide-treated HFO. Shows initial amount, pH, rate constants are presented along with reaction products and mechanism if observed

| CHC | Initial amount (µmol) | pH | k_{obs} | | Degradation byproducts | Degradation pathway |
			L g^{-1} hr^{-1}	R^2		
CF	0.0417	7	1.07E-04	0.61	None	-
TCE	0.0284	7	5.95E-04	0.30	None	-
TCE	0.0273	8	4.46E-05	0.61	None	-
TCE	0.0296	10	9.50E-05	0.77	None	-

CHAPTER 2

DEGRDATION OF SELECT CHLORINATED HYDROCARBONS BY HYDROXYL

RADICALS PRODUCED IN THE DARK BY OXYGENATION OF SODIUM

DITHIONITE-REDUCED HFO

2.1 BACKGROUND

2.1.1 Hydroxyl Radicals Production

The chemical reduction of O_2 to H_2O is a sequential multi-step process leading to

the formation of very short-lived and highly reactive transient species such as, superoxide

radical (O_2^{*-}), hydrogen peroxide (H_2O_2), and hydroxyl radicals (OH*), which are

collectively known as reactive oxygen species (ROS) (Zhang et al., 2016; Das and

Choudhary, 2014). Among the ROS species, OH* is considered a potent yet non-

selective oxidant that is capable of oxidizing a wide variety of organic and inorganic

species. OH* has been studied extensively for its application in engineered systems,

including wastewater treatment (Ebrahiem et al., 2017; Wols et al., 2013) and

remediation of recalcitrant compounds, such as chlorinated ethenes (Teel et al., 2001).

OH* also plays an important role in the environment, such as atmosphere (Levy, 1971)

and natural waters (Trusiak et al., 2018; Zhang et al., 2016).

In engineered systems, OH* can form via multiple pathways, including ozone-driven (e.g., peroxone process), UV-catalyzed (e.g. UV/H_2O_2), electrochemical (e.g., boron-doped diamond), and catalytic/Fenton's reactions (Miklos et al., 2018). In natural waters, the photochemical reaction of chromophoric dissolved organic matter (CDOM) and photo-Fenton reaction are considered as major pathways for OH* generation (Mopper and Zhou, 1990; Mostafa et al., 2013; Page et al., 2014). More recently, a light-independent 'dark production' of *OH in natural water has been reported (Minella et al., 2015; Page et al., 2013; Tong et al., 2016), in which reduced species, like DOM and Fe (II), have been shown to play a key role in donating electrons for oxygen reduction.

It has been shown that Fe(II) in iron mineral phases and in subsurface sediment porewater can produce *OH radicals by reaction with oxygen in the absence of light; examples include clays (Zeng et al., 2017), field sediments (Tong et al., 2016), mackinawite (Cheng et al., 2016), pyrite (Zhang et al., 2016a), simulated acid mine drainage (Zhu et al., 2017), and Fe(II)-coated zero valent iron (Ai et al., 2013). In certain studies (Zeng et al., 2017; Wang et al., 2017; Tong et al., 2016), sodium dithionite (SD) was employed to reduce structural ferric iron in sediments (oxides and clays) to ferrous form prior to study the *OH radical production by oxygenation. Tong et al. (2016) used SD to reduce structural ferric oxide coating on clays in sediments in order to assess its *OH radical production capacity.

However, the role of *OH radicals produced from dithionite-reduced iron oxides in CHC oxidation remains largely uninvestigated. In the present study, the hydroxyl radicals were generated by oxygenating dithionite-reduced hydrous ferric oxide (HFO),

in order to examine its potential of *in situ* oxidation of chlorinated ethenes in iron

reducing aquifers experiencing periodic influx of dissolved oxygen.

2.1.2 Iron Reduction by Sodium Dithionite

Sodium dithionite ($Na_2S_2O_4$) is a sulfur-containing reductant in alkaline condition

[$E_o^{1/2}$ =-1.12V] that dissociates rapidly into two sulfoxyl radicals ($SO_2^{\cdot-}$) that in turn can

reduce Fe(III) in sediment to Fe(II) (Amonette et al.,1994; Szecsody et al., 2004; Xie and

Cwiertny, 2010).

$$S_2O_{4aq}^{2-} \leftrightarrow 2SO_2^{\cdot-} \text{(in basic solution)} \tag{2.1}$$

$$SO_2^{\cdot-} + Fe(III) + H_2O \rightarrow Fe(II) + SO_3^{2-} + 2H^+ \tag{2.2}$$
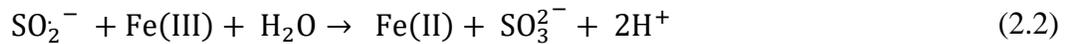
Overall, one mole of dithionite can reduce 2 moles of Fe (III) to Fe (II) (Equations

2.1 and 2.2 above), where the protons released during iron reduction (Equation 2.2) can

lower the pH to near neutral (Boparai et al., 2006).

2.1.3 OH* Production by Fe (II) Oxygenation

Burns et al. (2010) compiled the rate constants of Fe(II) oxidation when oxygen is

in excess. Equations 2.3-2.9 below show that O_2 reduction by Fe(II) is a three-step one

electron transfer sequential process. First, one Fe(II) reduces one O_2 molecule to form

superoxide radical, which is further reduced by second Fe(II) to produce hydrogen

peroxide, which in turn is also reduced by a third Fe(II) to form a hydroxyl radical

(Equations 2.3-2.5 below). Overall, 3 moles of electrons are needed to generate one mole

of *OH from reduction of one mole of O_2 (Yuan et al., 2018). As such 3 moles of Fe(II),

as an electron donor, is required to generate one mole of *OH, as follows (Burns et al., 2010):

$$Fe^{2+} + O_2 \leftrightarrow Fe^{3+} + O_2^{*-} \qquad k_1 = 13 \text{ M}^{-1}\text{s}^{-1}; k_{-1} = 1.5 * 10^8 \text{ M}^{-1}\text{s}^{-1} \qquad (2.3)$$

$$Fe^{2+} + O_2^{*-} \xrightarrow{2H^+} Fe^{3+} + H_2O_2 \qquad k_2 = 1 * 10^7 \text{ M}^{-1}\text{s}^{-1} \qquad (2.4)$$

$$Fe^{2+} + H_2O_2 \rightarrow Fe^{3+} + OH^* + OH^- \qquad k_3 = 7.6 * 10 \text{ M}^{-1}\text{s}^{-1} \qquad (2.5)$$
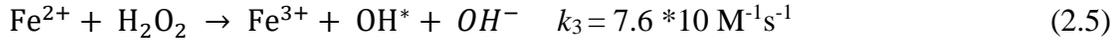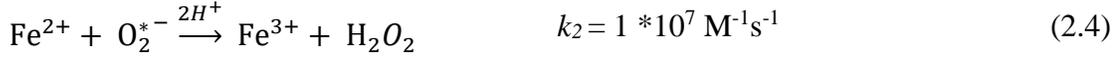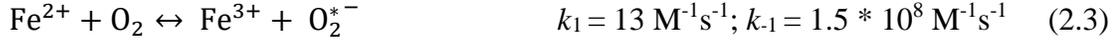
In terms of the rate constants, Equation 2.3 is a reversible reaction with a very fast kinetics for backward reaction (Burns et al., 2010). The reaction can move forward only at high Fe(II) concentrations and thus be a rate-limiting reaction. Equation 2.4 is also slower so, this also could be another rate-limiting step (Burns et al., 2010). Additional side-reactions are possible, such as oxidation of Fe(II) to Fe(III) by hydroxyl radical (Equation 2.6 below). Equations 2.7-2.9 below show additional reactions involving OH* that generate hydrogen peroxide and oxygen back in the system.

$$Fe^{2+} + OH^* \leftrightarrow Fe^{3+} + OH^- \qquad k_4 = 3.2 * 10^8 \text{ M}^{-1}\text{s}^{-1}; k_{-4} = 5 * 10^8 \text{ M}^{-1}\text{s}^{-1} \qquad (2.6)$$

$$O_2^{*-} + O_2^{*-} \xrightarrow{2H^+} H_2O_2 + O_2 \qquad k_5 \le 13 \text{ M}^{-1}\text{s}^{-1} \qquad (2.7)$$

$$O_2^{*-} + HOO^* \rightarrow H_2O_2 + O_2 \qquad k_6 = 1.02 * 10^8 \text{ M}^{-1}\text{s}^{-1} \qquad (2.8)$$

$$HOO^* + HOO^* \leftrightarrow H_2O_2 + O_2 \qquad k_7 = 8.6 * 10^8 \text{ M}^{-1}\text{s}^{-1} \qquad (2.9)$$
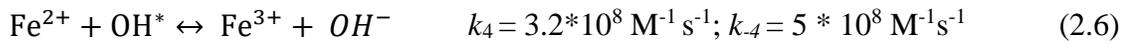
2.1.4 Oxidative Degradation of CHC by OH* Produced by Fe (II) Oxygenation

Hydroxyl radical [pK_a (*OH) = 11.9] is one of the strongest oxidants with a pH dependent standard reduction potential: +2.7V in acidic solution and +1.8V in neutral solution (Buxton et al, 1988). Recent studies have examined the mechanism of

chlorinated hydrocarbons (CHC) oxidation by *OH. Qiang and Huang (2008) proposed

TCE oxidation by hydroxyl radicals through dichloroacetic acid pathway, in which *OH

can attack and break the C-C double bond to give a sequence of two organic radicals (T_1

and T_2; Figure 2.1), which transform into dichloroacetic acid (DCAA). They suggested

that DCAA can further convert to CO_2 or can undergo partial degradation to other

chlorinated and non-chlorinated products. Pignatello et al., (1999) also observed DCAA

as reaction intermediate during TCE oxidation in photo-Fenton system.
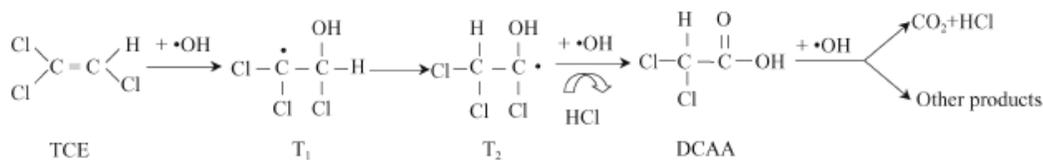
Figure 2.1: Mechanism of TCE oxidation by hydroxyl radicals (Qiang and Huang, 2008)

2.1.5 Research Objectives

The overall objective of the present study was to examine potential degradation of

select chlorinated ethenes employing a new technique for hydroxyl radical generation:

dark production of hydroxyl radicals by oxygenation of sodium dithionite (SD) reduced

hydrous ferric oxide (HFO). The specific objectives were as follows:

1. To examine the effect of aging of the SD reduced HFO on *cis*-1,2-dichloroethene
   degradation

2. To study the effect of initial amount of *cis*-1,2-dichloroethene on *cis*-1,2-
   dichloroethene degradation

3. To investigate the effect HFO: SD molar ratio on *cis*-1,2-dichloroethene
   degradation

4. To study the reaction kinetics of selected chlorinated CHC compounds: 1,1-dichloroethene, *cis*- 1,2-dichloroethene, *trans*-1,2-dichloroethene, tetrachloroethene, trichloroethene, and ethene

2.2 MATERIAL AND METHODS

2.2.1 Chemicals

Following chemicals were used as received: ferric chloride hexahydrate ($FeCl_3.6H_2O$, ACS grade, Ricca Chemical Company), sodium dithionite ($Na_2S_2O_4$, technical grade; Sigma-Aldrich). Organics used included: 1,1-dichloroethene (1,1-DCE, Tokyo Chemical Industries, 99%), *cis*-dichloroethene (*cis*-1,2-DCE, Fischer Scientific, 97%), *trans*-dichloroethene (*trans*-1,2-DCE, Fisher Scientific, 97%), tetrachloroethene (PCE) and trichloroethene (TCE, Fisher Scientific, 97%). High purity gases (He, N_2, H_2, air; zero grade) were obtained from Praxair, Dayton, OH. Gaseous ethene was obtained from Weiler Wielding Co., Inc. (purity: 99.9%).

Following materials were used: 72mL borosilicate serum bottles (Cat# 223746, Wheaton), PTFE-lined butyl stoppers (Cat# 73811T-21, Kimble-Chase), aluminum crimps and disposable plastic syringes. Lab equipment used include anaerobic chamber (Coy Lab, MI), rotatory shaker (Glass-Col, IN), pH meter (Denver Instrument; AP10) and Vortex Genie 2 lab mixer (Fisher).

2.2.2 Bench-scale Experimental Setup

Nanoscale HFO was synthesized by neutralizing 0.1 M ferric chloride hexahydrate ($FeCl_3.6H_2O$) with 0.3 M NaOH (Zachara et al., 1998). The NaOH solution was added dropwise until the pH of the HFO suspension reached ~7.2-7.3. This HFO was allowed to react overnight on a magnetic stir plate, and then was repeatedly washed with deionized water until the electrical conductivity of the supernatant was less than 250 μS cm^{-1}.

Batch reactors containing 25 mM HFO (1.4 g/L) were prepared in 72 mL glass serum bottles (Cat# 223746, Wheaton, NJ) and sealed with PTFE-lined stoppers (Cat# 73811T-21, Kimble Chase, NJ), and then deoxygenated by bubbling high-purity N_2 gas individually for 20 min. each (see section 1.2.2 for additional details). An additional step for removing trace levels of O_2 from the reactors was employed by passing the high-purity N_2 gas stream through a glass tube filled heated copper turnings. The reactors were then transferred to an anaerobic chamber (Coy Lab, USA; ~2.5% H_2 and balance N_2) and then were allowed to equilibrate overnight. On the next day, 1 mL of supernatant fluid was removed from the reactors by a syringe and replaced with 1 mL of sodium dithionite solution. An aqueous dithionite reagent (~260 mM) was freshly prepared by weighing and dissolving 1.33 g of sodium dithionite in 25 mL deoxygenated deionized water inside the anaerobic chamber. Amending the batch reactors with the dithionite reagent solution immediately turned the color of the solid phase HFO to a dark brown solid suggesting reduction of Fe(III) in HFO to Fe(II). The HFO to SD ratio was nominally 4.7:1 in most experiments; see section 2.2.2.2 for the effect of variations in HFO:SD ratio on *cis*-1,2-DCE degradation.

The reactors were then brought out of the anaerobic chamber and wrapped with aluminum foil and equilibrated on end-over end rotator (Cat 099A; Glas Col, IN) at 45 rpm, typically for 16 hours. However, the HFO equilibration time with SD was varied to examine its effect on *cis*-1,2-DCE degradation by OH*; see section 2.2.2.1). The reactors were then oxygenated by bubbling with a gentle stream of high-purity O_2 gas for ~2 min, via a stainless-steel needle piercing through the stoppers. This setup also had a vent needle pierced through the stopper to maintain atmospheric pressure in the reactors.

High concentration CHC stock solution was prepared in a 160 mL serum bottle containing Milli-Q water by injecting following amount of pure phase CHCs: *cis*-1,2-DCE (365 µL), *trans*-1,2-DCE (370 µL), 1,1-DCE (385 µL), TCE (100 µL) and PCE (12 µL). Immediately after oxygenation, an individual CHC stock solution (25-200 µL) was injected into the reactors using a gastight syringe (Hamilton, Reno, NV). The reactors were then agitated vigorously on a vortex mixer for 30 seconds and then placed on rotary shaker for end-over-end continual mixing at 45 rpm. A DI control (oxygenated deionized water control with CHC) was also run in each experiment. Headspace samples were withdrawn using a gastight syringe every half an hour upto six hours and an additional sample at 7th hour. The headspace samples were analyzed by gas chromatography.

Further, the role of following experimental parameters on CE degradation was examined, as described below:

2.2.2.1 Effect of Oxygen on cis-1,2-DCE Degradation

The effect of presence of oxygen was examined on *cis*-1,2-DCE. The reactors were prepared at 4.7:1 HFO:SD molar ratio and were equilibrated for 16 hours as in

section 2.2.2. One set of triplicate reactors were oxygenated for 2 minutes before addition of 200 µL of *cis*-1,2-DCE stock solution while in the other set of triplicate reactors same amount of *cis*-1,2-DCE stock solution was added without oxygenation.

2.2.2.2 Effect of Dithionite-Reduced HFO aging on cis-1,2-DCE Degradation

The effect of aging of the solid phase formed by reduction of HFO by dithionite was examined on *cis*-1,2-DCE. The durations of reactor aging (equilibration) were 3, 16, and 302 hrs (7 days) on the rotator under well-mixed conditions. The equilibration time represent the interval between addition of dithionite to HFO and oxygenation of the reactors. Immediately after oxygenation, 200 µL of *cis*-1,2-DCE stock solution was added. All other experiments were done with 16-hour maturation of the phase based on two things: easiness of working and reduction in the standard deviation between the reactors.

2.2.2.3 Effect of HFO: SD Ratio on Cis-1,2-DCE Degradation

The *OH radicals generated may depend on the amount of Fe(II) in the oxygen rich system. Fe (II) can be varied in two ways, such as varying the amount of HFO, or by varying the amount of SD. In this study, we varied the amount of SD keeping the amount of HFO constant. Three HFO:SD molar ratios were investigated: 4.7:1 (25 mM HFO:5.3 mM SD), 2.4:1 (25 mM HFO: 10.6 mM SD) and 6.8:1 (25mM HFO: 2.7 mM SD). The HFO reactors were prepared, deoxygenated and equilibrated as in section 2.2.2. The difference in these three reactors were: for 4.7:1 ratio reactor,1 mL of supernatant was removed, for 2.4:1 reactor, 2 mL of supernatant was removed, and for 9.4:1 (0.25 mL of supernatant was removed. An equivalent amount of SD stock was added to reactors in

each of above experiments. The reactors were oxygenated as in section 2.2.2 and then 200 µL of *cis*-1,2-DCE stock solution was added.

2.2.2.4 Effect of Initial Amount of cis-1,2-DCE on cis-1,2-DCE Degradation

Three initial amounts of *cis*-1,2-DCE were studied: 5.47 µmol, 1.72 µmol and 0.72 µmol. For this set of experiments, the reactors were prepared using 4.7:1 HFO:SD molar ratio followed by 16 hours of maturation of the solid phase after SD addition to HFO. Following amounts of *cis*-1,2-DCE stock solution were added immediately after oxygenation: 5.47 µmol (200 µL), 1.72 µmol (60 µL) and 0.72 µmol (25 µL).

2.2.2.5 Selected compounds

Five chlorinated ethenes were studied*: cis*-1,2-DCE, *trans*-1,2-DCE, 1,1-DCE, TCE and PCE along with ethene. The reactors were prepared at 4.7:1 HFO:SD molar ratio, aged for 16 hours and oxygenated for 2 minutes as in section 2.2.2. The amount of these compounds added to the reactors varied and was decided based on its solubility in water, linear range of calibration curve, saturation of the detector, and minimum detection limit of the employed method. Following initial volume were added from respective stocks discussed in section 2.2.2: 1,1-DCE (80 µL), *cis*-1,2-DCE (200 µL), *trans*-1,2-DCE (200 µL), TCE (50 µL) and PCE (50 µL). For ethene experiment, 150 µL of gaseous ethene was added from ethene gas tank. These volumes translated to the following amount: 1,1-DCE (2.26 µmol), *cis*-1,2-DCE (5.47 µmol), *trans*-1,2-DCE (5.46 µmol), TCE (0.38 µmol), PCE (0.035 µmol) and ethene (6.09 µmol).The amount of 1,1-DCE, TCE and PCE were smaller because of the saturation of the ECD detector.

2.2.3 Analytical methods

CHCs and degradation products were analyzed in a gas chromatograph (7890 GC system; Agilent Technologies) equipped with electron capture detector (ECD) and flame ionization detector (FID). CHCs were separated on HP 624 (30 m x 0.32 mm x 0.25 µm; Agilent Technologies) capillary column and were visible on ECD. Non-chlorinated hydrocarbons were separated on Gas Pro capillary column (30 m x 0.32 mm x 0.25 µm, Agilent Technologies) and were visible on FID. Helium was used as a carrier gas at a constant flow of 2.5 mL min^{-1}. The GC method was split/splitless inlet = 250 °C, oven temperature = 100 °C (isothermal). Nitrogen gas (N_2) was used as the makeup gas with flow rate of 25 mL min^{-1} for ECD. The flow rate for H_2 and air was 450 and 30 mL min^{-1} respectively for FID.

2.2.4 Data Treatment

The peak area values obtained from GC-ECD/FID was converted to chemical amounts (µmol) using slope of the calibration curve. The values reported in amount-time charts are averages of triplicate reactors, and the standard deviations are shown as error bars in the charts. The apparent lack of error bars in the figures indicates that the error bars are very small and are hidden behind the size of the data point symbol.

The average amount of the chemical obtained vs. time was plotted in MS Excel and a pseudo first-order rate model was fitted to the amount-time data set; the value of the exponent of the fitted exponential decay equation provides the observed rate constant of degradation (k_{obs}). The data plots often showed a faster initial kinetics, followed by slower kinetics; on this basis, the degradation curves were divided into two phases, and

the rate constants were estimated for an initial fast phase (k_{obs1}) and a slower second

phase (k_{obs2}). Data from the DI control reactor are included in the charts in Appendix A.

2.3 RESULTS AND DISCUSSIONS

2.3.1 General Observation

An initial delay of 0.5-1.5 hour before the onset of CHC degradation by

dithionite-treated HFO was typically observed for all experiments (except with HFO:SD

molar ratio = 9.4:1, maturation ≥ 7 hours) (Table 2.1). Minella et al. (2015) reported

hydroxyl radical production with a 10 minutes induction period after contact with

atmosphere in bottom water samples from lakes. The cause of this delay was not

reported. No other work is identified with any induction period. This should be reflective

of the employed experimental conditions; however, it was not dependent on HFO:SD

molar ratio, aging, different compounds and initial amount (Table 2.1). One possible

explanation is the smaller forward rate constant in Equation 2.3. For kinetics analysis, the

curve after the induction period has been considered as the degradation curve and is used

in fitting pseudo first order model.

During the induction period, an increase in peak area compared to what was

initially injected was observed followed by a gradual decrease in peak area towards initial

value before initiation of degradation. Although, the exact reason behind this behavior

remains elusive, one possible explanation could be, the system didn't reach equilibrium

between headspace and aqueous phase until that time. Another reason could be some

reaction intermediates may be causing elevated partitioning of the compounds into headspace. This however needs detailed study for confirmation.

2.3.2 Effect of Oxygen on *cis*-1,2-DCE Degradation by SD-Reduced HFO

The degradation of *cis*-1,2-DCE by dithionite-treated HFO was observed only in presence of oxygen (Figure 2.1A). At 7 hours, oxygenated system had only 6% of initial *cis*-1,2-DCE remaining whereas the non-oxygenated reactors had 106%. This clearly shows that oxygen is a key factor for the reactivity of this system. The reaction of Fe (II) formed by reduction of HFO by SD with oxygen produces *OH radical which is capable of oxidizing double bonded chlorinated hydrocarbons (Burns et al., 2010; Qiang and Huang, 2008).

2.3.3 Effect of Aging of SD-Reduced HFO on *cis*-1,2-DCE Degradation

cis-1,2-DCE degradation rate constant did not vary due to variation in the maturation period (3 hours: k_{obs1}= 0.65 hr^{-1}; k_{obs2}= 0.37hr^{-1}; 16 hours: k_{obs1}= 0.65 hr^{-1}; k_{obs2}= 0.37hr^{-1}; 7 days: k_{obs1}= 0.64 hr^{-1}; k_{obs2}= 0.26hr^{-1}) (Table 2.1; Figure 2.1B). This relatively constant k_{obs1} suggests that there is no substantial change in the electron donating capacity of the system over the period.

2.3.4 Effect of Initial Amount of *cis*-1,2-DCE on *cis*-1,2-DCE Degradation

In 0.72 µmol experiment, no appreciable peak was observed in the latter half of the experiment and hence only k_{obs1} is discussed. *cis*-1,2-DCE degradation rate constants did not vary with the initial amount of *cis*-1,2-DCE (5.47 µmol: k_{obs1}= 0.65 hr^{-1}; 1.72 µmol k_{obs1}= 0.64; 0.70 µmol: k_{obs1}= 0.68 hr^{-1}) (Table 2.1; Figure 2.2A). This relatively

constant k_{obs1} indicates that the degradation is independent of the initial amount of contaminant in the observed range. This also suggests that the difference in reactivity of different compounds in section 2.3.5 is not due to their differing initial amount but is due to their intrinsic reactivity.

2.3.5 Effect of HFO: SD Ratio on *cis*-1,2-DCE Degradation

cis-1,2-DCE degradation rate constants decreased with decreasing amount of dithionite (4.7:1 ratio: k_{obs1}= 0.65 hr^{-1}; k_{obs2}= 0.37hr^{-1}; 2.4:1 ratio: k_{obs1}= 0.83 hr^{-1}; k_{obs2}= 0.54 hr^{-1}; 9.4:1 ratio: k_{obs1}= 0.06 hr^{-1}; k_{obs2}= 0.01hr^{-1}) (Table 2; Figures 2.2, 2.4 and 2.5). The decrease in rate constants with decrease in dithionite amount is expected; with smaller amount of dithionite, smaller fraction of Fe (III) is reduced or lesser amount of Fe (II) is formed. Stoichiometrically, the amount of Fe (II) formed should be twice for HFO:SD molar ratio of 2.4:1 when compared to 4.7:1 and half for HFO: SD molar ratio of 9.4:1 when compared to 4.7:1. However, no such proportional changes in rate constant is observed; the ratio of k_{obs1} (normalized to k_{obs1} for 9.4:1) for 2.4:1, 4.7:1 and 9.4:1 HFO:SD molar ratio are 13.8:10.8:1 indicating an order of magnitude lower k_{obs1} for 9.4:1 when compared to other two ratios.

Gorski et al. (2010) observed similar non-proportional changes in nitrobenzene reduction rates with magnetite; the reduction rates decreased by five orders of magnitude when the ratio of structural Fe (II)/structural Fe (III) was decreased from 0.50 to 0.31. They suggested that models based on diffusion only e.g. core-shell diffusion model of Fe (II) migrating towards the surface and reacting may not provide complete picture and

recommended considering both redox and Fe (II) diffusion processes in explaining such behavior.

2.3.6 Degradation of Selected Chlorinated Ethenes by Oxygenation of SD-Reduced HFO

2.3.6.1 1,1-DCE

1,1-DCE degradation started after 1-hour initial lag with faster initial degradation (k_{obs1} = 2.06 hr^{-1}) followed by a slower reaction afterwards (k_{obs2} = 0.80 hr^{-1}) (Table 2.1; Figure 2.6 B). Degradation by-products (chlorinated and non-chlorinated hydrocarbons) were not observed.

2.3.6.2 trans-1,2-DCE

trans-1,2-DCE degradation started after 1-hour initial lag with faster initial degradation (k_{obs1}= 0.56 hr^{-1}) and slower reaction afterwards (k_{obs2}= 0.26 hr^{-1}) (Table 2.1; Figure 2.7 B). Degradation by-products (chlorinated and non-chlorinated hydrocarbons) were not observed.

2.3.6.3 cis-1,2-DCE

cis-1,2-DCE degradation started after 1-hour initial lag with faster initial degradation (k_{obs1}= 0.65 hr^{-1}) and slower reaction afterwards (k_{obs2}= 0.37hr^{-1}) (Table 2.1; Figure 2.2 B). Degradation by-products (chlorinated and non-chlorinated hydrocarbons) were not observed.

2.3.6.4 TCE

TCE degradation started after 0.5-hour initial lag with faster initial degradation (k_{obs1}= 1.82 hr^{-1}) degradation until 2 hours; the reaction slowed afterwards (k_{obs2}= 0.68 hr^{-1}). Degradation by-products (chlorinated and non-chlorinated hydrocarbons) were not observed.

2.3.6.5 PCE

PCE degradation started after 1.5-hour initial lag with faster (k_{obs1}= 1.08 hr^{-1}) degradation until 2.5 hour; the reaction slowed afterwards (k_{obs2}= 0.50 hr^{-1}). Degradation by-products (chlorinated and non-chlorinated hydrocarbons) were not observed.

2.3.6.6 Ethene

Ethene degradation started after 1.5-hour initial lag with faster (k_{obs1}= 0.28 hr^{-1}) degradation until 2.5 hour; the reaction slowed afterwards (k_{obs2}= 0.13 hr^{-1}). Degradation by-products (chlorinated and non-chlorinated hydrocarbons) were not observed.

2.3.6.7 Comparison of Rate Constants

The observed pattern for k_{obs1} and k_{obs2} were: 1,1-DCE > TCE > PCE > *trans*-1,2-DCE > *cis*-1,2-DCE > ethene (Table 2.1; Figures 2.4 A, 2.4 B and 2.5). The reactivity order of three DCE isomers is in good agreement to that observed by Tuazon et al., (1988) in homogenous gas phase reaction of chlorinated ethenes with hydroxyl radicals; the ratio of reactivity of three DCE isomers (normalized to *trans*-1,2-DCE) was 4.24:1.56:1.00 which is similar to that observed in our experiments for k_{obs1} 4.57:1.16:1.00. Interestingly, Doughty et al., (2005) also observed similar order of

reactivity of three DCE isomers in a biological system (co-oxidation by butane grown *Pseudomonas butanovora* with lactate as external electron donor).

Likewise, ratio of k_{obs1} of PCE: TCE (0.59) reported in Haag and Yao (1992) in photo-Fenton system is similar to that observed in our experiments (0.54). They suggested such relative rates of oxidation can be used in verifying the production of involvement of hydroxyl radicals. So, such comparable ratios of rate constant with Tuazon et al., (1988) and Haag and Yao (1992) suggests that the degradation in our experiment is due to hydroxyl radicals.

As the number of chlorine atoms increase, the reactivity is affected by negative induction effect: chlorine is highly electronegative and exerts strong electron withdrawing effect thus decreasing the electron density at carbon- carbon double bond making the electron pair less available for oxidation (Qiang and Huang, 2008; Yan and Schwartz, 1999). Also, with increasing number of chlorine atoms, the steric hindrance for attack increases, however, the inductive effect of chlorine substituent may be more important than their steric hindrance (Vogel et al., 1987). This explains the decrease in reactivity order:1,1-DCE>TCE>PCE. However, the lower reactivity of ethene cannot be explained based on this.

When compared with all studied compounds, ethene had the lowest reactivity which contrasts the above explanation based on induction effect. Lee (1982) (as cited in Yan and Schwartz, 2009) suggested if halogen atoms are present at an oxidation site, it can aid in degradation of hydrocarbons. This may be the reason of higher k_{obs} observed for all chlorinated ethenes when compared to ethene.

The observed order among three DCE isomers (1,1-DCE > *cis*-1,2-DCE > *trans*-1,2-DCE) may be related to the position of chlorine atom as all of them have two chlorine atoms. Two chlorine atoms on α-carbon (1,1-DCE) showed higher reactivity than two atoms distributed among α and β positions. Furthermore, two chlorine atoms on same side of molecule (*cis*-1,2-DCE) showed higher reactivity than on the opposite side (*trans*-1,2-DCE). This can be explained based on stability of the molecule related to strong Van Der Waals force of repulsion between two chlorine atoms. The more near the chlorine atoms are, the bigger is the instability due to this repulsive force. In line with this, *trans*-isomers are reported to be more stable than *cis*-isomers in alkenes (Yan and Schwartz, 1999).

2.4. CONCLUSIONS

1. The maturation of the solid phase formed by reduction of HFO by dithionite did not affect the rate of degradation of *cis*-1,2-DCE between 3 hours and 7 days.

2. Initial amount of *cis*-1,2-DCE between 5.47 µmol and 0.72 µmol did not affect its rate of degradation.

3. k_{obs1} of *cis*-1,2-DCE degradation increased non-proportionately with increase in concentration of dithionite. Effect on *cis*-1,2-DCE degradation rates were investigated at three HFO:SD molar ratios: 9.4:1, 4.7:1 and 2.4:1 (SD concentration is increasing by a factor of ~2 successively); The ratios of k_{obs1} were 1:10.8:13.8 (normalized to k_{obs1} of 9.4:1) for these three ratios respectively indicating a magnitude of order increase between 9.4:1 to 4.7:1 while it increased by 1.27 times between 4.7:1 to 2.4:1.

4. Observed order of k_{obs1} was :1,1-DCE >TCE > PCE > *cis*-1,2-DCE > *trans*-1,2-DCE and ethene. The decrease in the reactivity order (1,1-DCE >TCE> PCE) may be explained based on strong inductive effect exerted by successively increasing number of chlorine atoms. Surprisingly, ethene with no chlorine substituents showed the least reactivity. The ratio of rate constants observed are consistent to that observed with hydroxyl radicals generated from other methods. The order for DCE isomers 1,1-DCE> *cis*-1,2-DCE > *trans*-1,2-DCE may be explained based on position of the chlorine substituents.

REFERENCES

Amonette, J. E., Szecsody, J. E., Schaef, H. T., Templeton, J. C., Gorby, Y. A. and Fruchter, J. S. (1994) Abiotic reduction of aquifer materials by dithionite: a promising in-situ remediation technology. *In 33rd Hanford Symposium on Health and the Environment - In-Situ Remediation: Scientific Basis for Current and Future Technologies,* Richland, Washington.

Boparai, H.K., Shea, P.J., Comfort, S.D. and Snow, D.D. (2006) Dechlorinating chloroacetanilide herbicides by dithionite-treated aquifer sediment and surface soil. *Environmental Science & Technology, 40*, 3043-3049.

Cheng, D., Yuan, S., Liao, P. and Zhang, P. (2016) Oxidizing impact induced by mackinawite (FeS) nanoparticles at oxic conditions due to production of hydroxyl radicals. *Environmental Science & Technology, 50*, 11646-11653.

Das, K. and Roychoudhury, A., (2014) Reactive oxygen species (ROS) and response of antioxidants as ROS-scavengers during environmental stress in plants. *Frontiers in Environmental Science, 2*, 1-13.

Doughty, D.M., Sayavedra-Soto, L.A., Arp, D.J. and Bottomley, P.J. (2005) Effects of dichloroethene isomers on the induction and activity of butane monooxygenase in the

alkane-oxidizing bacterium "Pseudomonas butanovora". *Applied and Environmental Microbiology, 71*, 6054-6059.

Ebrahiem, E.E., Al-Maghrabi, M.N. and Mobarki, A.R. (2017) Removal of organic pollutants from industrial wastewater by applying photo-Fenton oxidation technology. *Arabian Journal of Chemistry, 10*, S1674-S1679.

Gorski, C.A., Nurmi, J.T., Tratnyek, P.G., Hofstetter, T.B. and Scherer, M.M. (2010) Redox behavior of magnetite: Implications for contaminant reduction. *Environmental Science & Technology, 44,* 55-60.

Haag, W.R. and Yao, C.C.D. (1992) Rate constants for reaction of hydroxyl radicals with several drinking-water contaminants. *Environmental Science & Technology, 26*, 1005-1013.

Levy, H. (1971) Normal Atmosphere - Large radical and formaldehyde concentrations predicted. *Science, 173,* 141-143.

Lee, D.G. (1982) Phase *trans*fer assisted permanganate oxidations. In: Trahanovsky, W.S. Ed., Oxidation in Organic Chemistry, Part D, Chap. 2. 147–206. Academic Press, New York.

Liu, X.X., Yuan, S.H., Tong, M. and Liu, D. (2017) Oxidation of trichloroethylene by the hydroxyl radicals produced from oxygenation of reduced nontronite. *Water Research, 113*, 72-79.

Miklos, D.B., Remy, C., Jekel, M., Linden, K.G., Drewes, J.E. and Hubner, U. (2018) Evaluation of advanced oxidation processes for water and wastewater treatment - A critical review. *Water Research, 139,* 118-131.

Minella, M., De laurentiis, E., Maurino, V., Minero, C. and Vione, D. (2015) Dark production of hydroxyl radicals by aeration of anoxic lake water. *Science of the Total Environment, 527,* 322-327.

Mopper, K. and Zhou, X.L. (1990) Hydroxyl radical photoproduction in the sea and its potential impact on marine processes. *Science, 250*, 661-664.

Mostofa, K. M., Liu, C. Q., Sakugawa, H., Vione, D., Minakata, D., Saquib, M., & Mottaleb, M. A. (2013). Photoinduced generation of hydroxyl radical in natural waters. *In Photobiogeochemistry of Organic Matter* (pp. 209-272). Springer, Berlin, Heidelberg.

Page, S.E., Logan, J.R., Cory, R.M. and McNeill, K. (2014) Evidence for dissolved organic matter as the primary source and sink of photochemically produced hydroxyl radical in arctic surface waters. *Environmental Science-Processes & Impacts, 16,* 807-822.

Pignatello, J.J., Liu, D. and Huston, P. (1999) Evidence for an additional oxidant in the photoassisted Fenton reaction. *Environmental Science & Technology, 33,* 1832-1839.

Qiang, Z., Ben, W. and Huang, C.P., 2008. Fenton process for degradation of selected chlorinated aliphatic hydrocarbons exemplified by trichloroethylene, 1, 1-dichloroethylene and chloroform. *Frontiers of Environmental Science & Engineering in China, 2*(4), 397-409.

Szecsody, J.E., Fruchter, J.S., Williams, M.D., Vermeul, V.R. and Sklarew, D. (2004) In situ chemical reduction of aquifer sediments: Enhancement of reactive iron phases and TCE dechlorination. *Environmental Science & Technology, 38,* 4656-4663.

Teel, A.L., Warberg, C.R., Atkinson, D.A. and Watts, R.J. (2001) Comparison of mineral and soluble iron Fenton's catalysts for the treatment of trichloroethylene. *Water Research, 35,* 977-984.

Tong, M., Yuan, S., Ma, S., Jin, M., Liu, D., Cheng, D., Liu, X., Gan, Y. and Wang, Y. (2016) Production of abundant hydroxyl radicals from oxygenation of subsurface sediments. *Environmental Science & Technology, 50,* 214-221.

Yan, Y.E. and Schwartz, F.W. (1999) Oxidative degradation and kinetics of chlorinated ethylenes by potassium permanganate. Journal of Contaminant Hydrology, 37(3-4), 343-365.

Yuan, S., Liu, X., Liao, W., Zhang, P., Wang, X. and Tong, M. (2018) Mechanisms of electron *trans*fer from structrual Fe (II) in reduced nontronite to oxygen for production of hydroxyl radicals. *Geochimica et Cosmochimica Acta*, *223,* 422-436.

Trusiak, A., Treibergs, L.A., Kling, G.W. and Cory, R.M. (2018) The role of iron and reactive oxygen species in the production of CO_2 in arctic soil waters. *Geochimica Et Cosmochimica Acta, 224,* 80-95.

Tuazon, E.C., Atkinson, R., Aschmann, S.M., Goodman, M.A. and Winer, A.M. (1988) Atmospheric reactions of chloroethenes with the OH radical. *International Journal of Chemical Kinetics, 20*, 241-265.

Vogel, T.M., Criddle, C.S. and McCarty, P.L. (1987) *Trans*formations of halogenated aliphatic-compounds. *Environmental Science & Technology, 21*, 722-736.

Wols, B.A., Hofman-Caris, C.H.M., Harmsen, D.J.H. and Beerendonk, E.F. (2013) Degradation of 40 selected pharmaceuticals by UV/H_2O_2. *Water Research, 47,* 5876-5888.

Xie, Y. and Cwiertny, D.M. (2010) Use of dithionite to extend the reactive lifetime of nanoscale zero-valent iron treatment systems. *Environmental Science & Technology, 44,* 8649-8655.

Zachara, J. M., Fredrickson, J. K., Li, S. M., Kennedy, D. W., Smith, S. C. and Gassman, P. L. (1998). Bacterial reduction of crystalline Fe^{3+} oxides in single phase suspensions and subsurface materials. *American Mineralogist, 83(11)*, 1426-1443.

Zeng, Q., Dong, H.L., Wang, X., Yu, T. and Cui, W.H. (2017) Degradation of 1, 4-dioxane by hydroxyl radicals produced from clay minerals. *Journal of Hazardous Materials, 331*, 88-98.

Zhang, P., Yuan, S. and Liao, P. (2016a) Mechanisms of hydroxyl radical production from abiotic oxidation of pyrite under acidic conditions. *Geochimica Et Cosmochimica Acta, 172,* 444-457.

Zhang, T., Hansel, C.M., Voelker, B.M. and Lamborg, C.H. (2016) Extensive Dark Biological Production of Reactive Oxygen Species in Brackish and Freshwater Ponds. *Environmental Science & Technology, 50,* 2983-2993.

Zhu, J., Zhang, P., Yuan, S., Liao, P., Qian, A., Liu, X., Tong, M. and Li, L. (2017) Production of hydroxyl radicals from oxygenation of simulated amd due to $CaCO_3$-induced pH increase. *Water Research, 111,* 118-126.
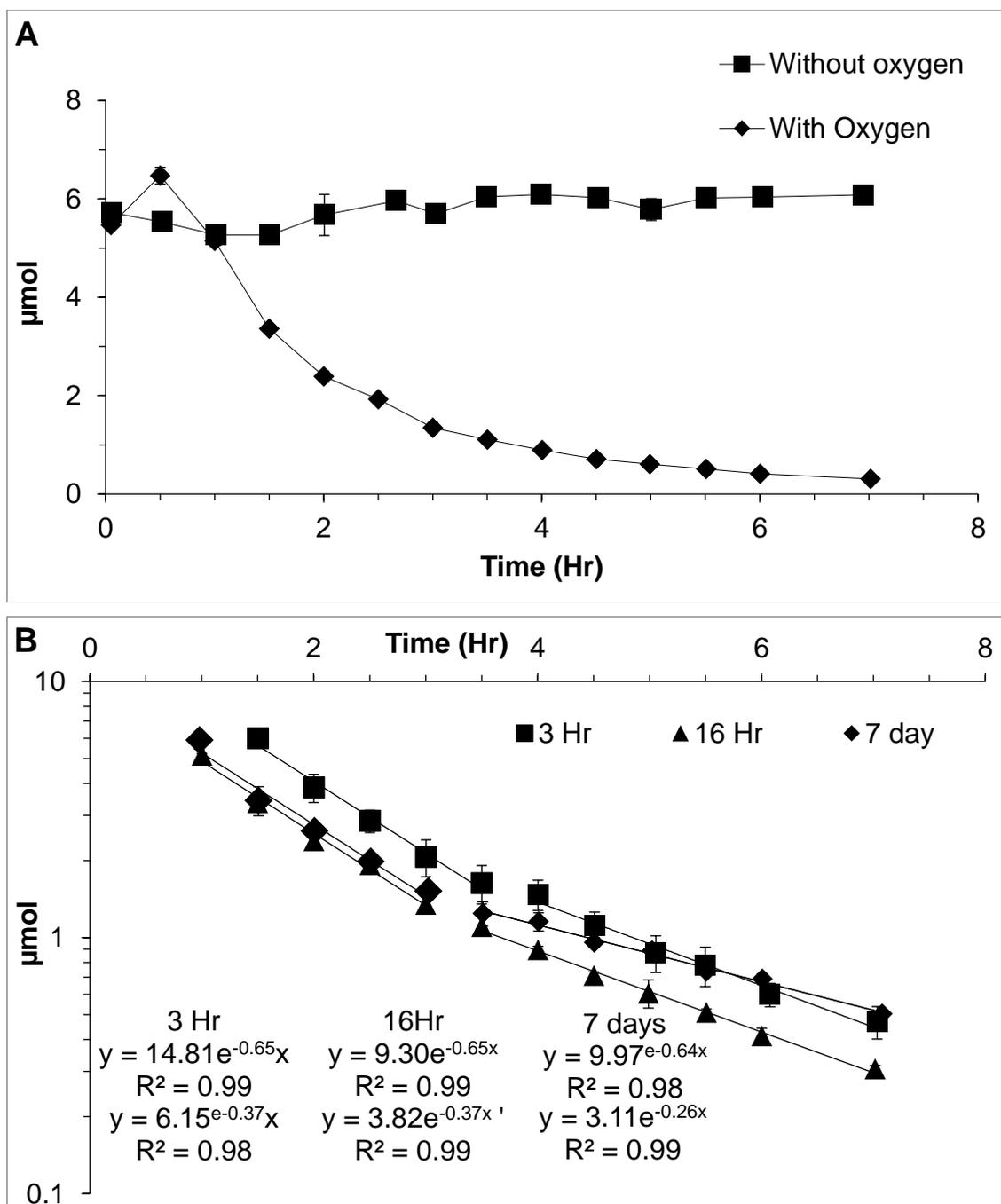
Figure 2.2: (A) *cis*-1,2-DCE degradation with and without oxygenation. Experimental conditions: HFO:SD molar ratio = 4.7:1; reactor equilibrated to age: 16-hours (B) *cis*-1,2-DCE degradation by oxygenation of SD reduced HFO for variable ages. Experimental conditions: HFO:SD 4.7:1 molar ratio, 2 minutes oxygenation with pure oxygen
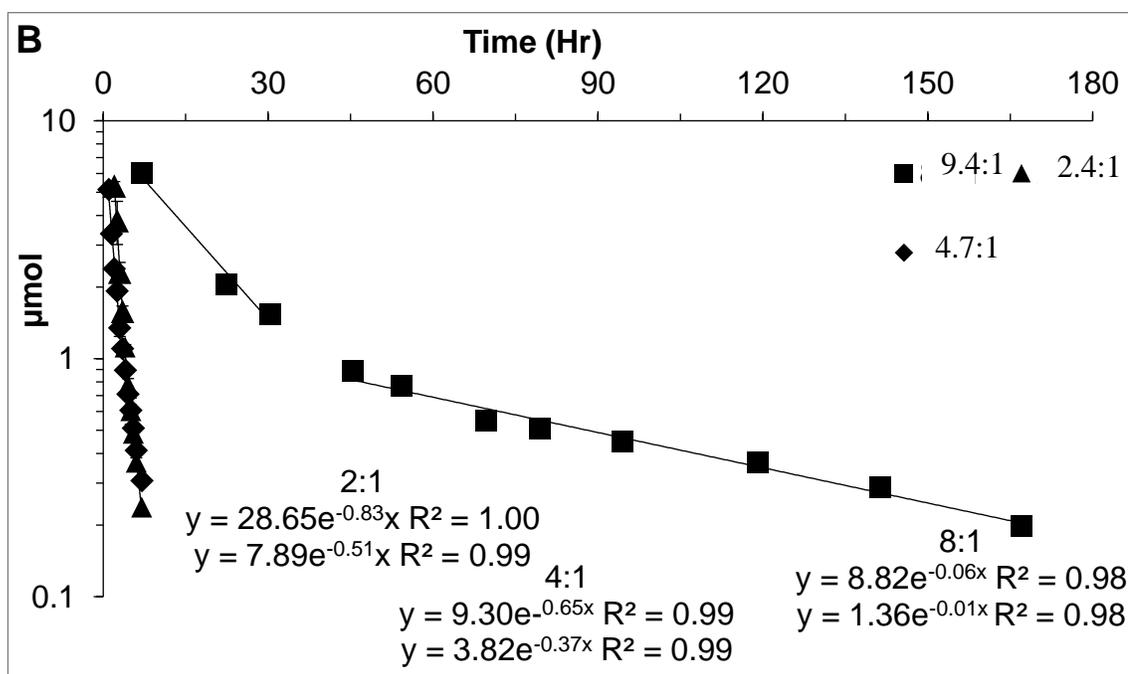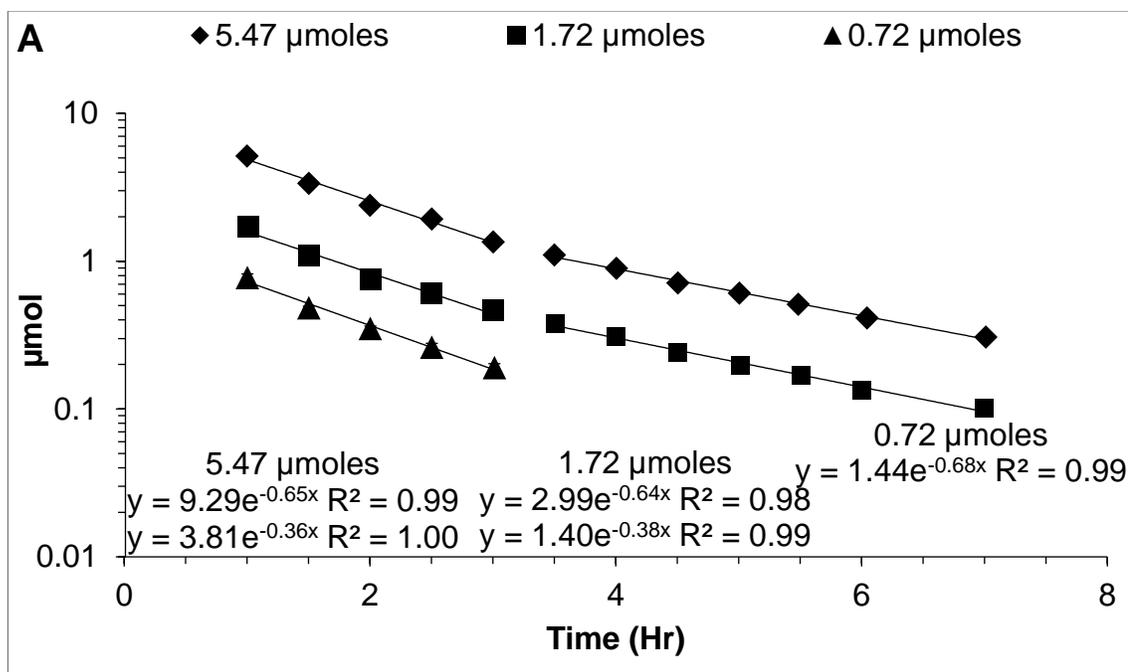
Figure 2. 3 (A) *cis*-1,2-DCE degradation rates for variable initial amounts (5.47 µmol, 1.72 µmol and 0.72 µmol). Experimental conditions: HFO:SD 4.7:1 molar ratio, Age: 16 hours, 2 minutes oxygenation with pure oxygen (B) *cis-* DCE degradation by oxygenation of SD reduced HFO at different HFO:SD molar ratios (2.4:1,4.7:1 and 9.4:1). Experimental conditions: Age: 16 hours, 2 minutes oxygenation with pure oxygen.
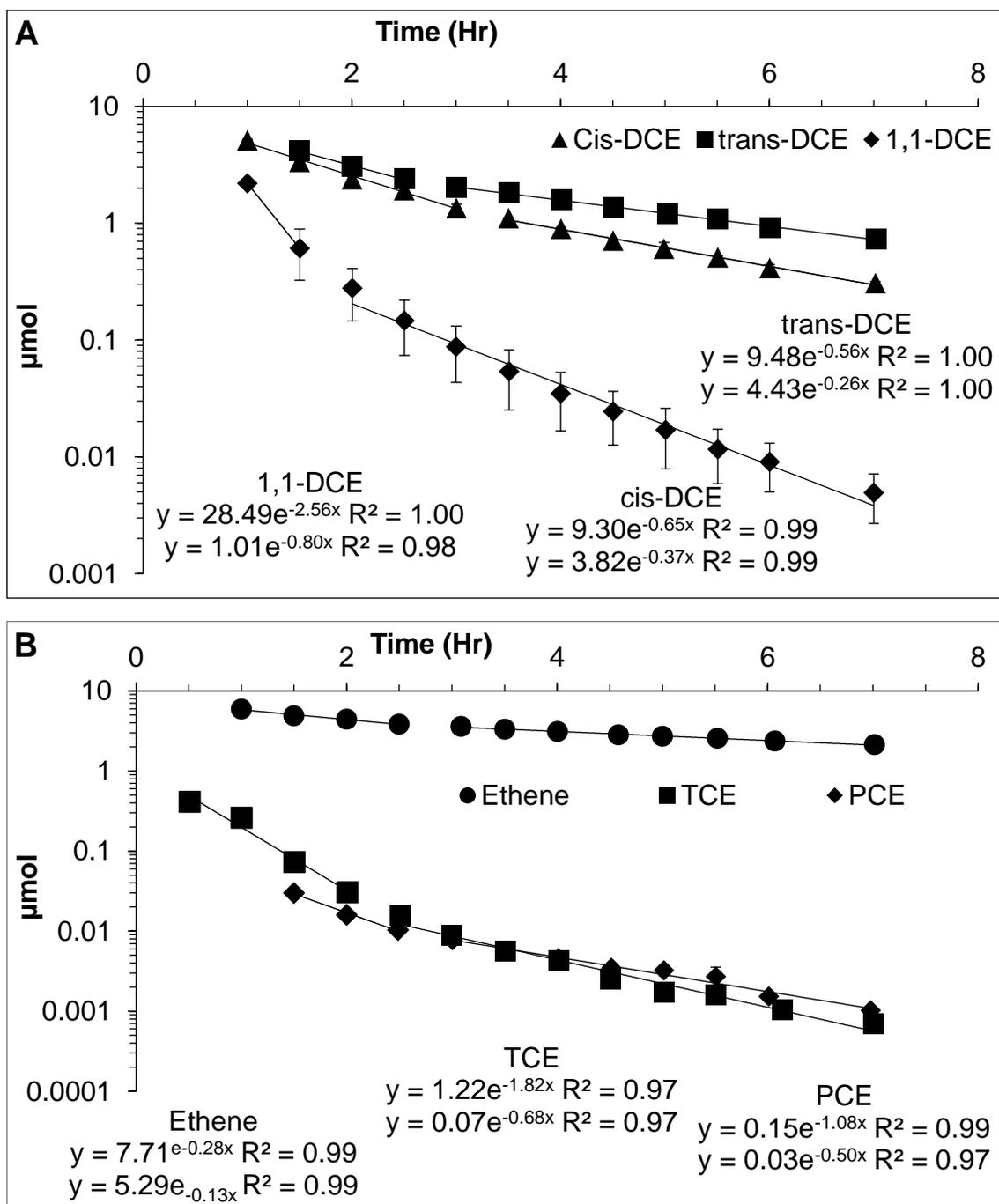
Figure 2.4 (A) Degradation of three DCE isomers by oxygenation of SD reduced HFO (B) Degradation of TCE, PCE and Ethene by oxygenation of SD reduced HFO. Experimental conditions: (for both A and B) HFO:SD 4.7:1 molar ratio, Age: 16 hours, 2 minutes oxygenation with pure oxygen; error bars indicate standard deviation among triplicate reactors
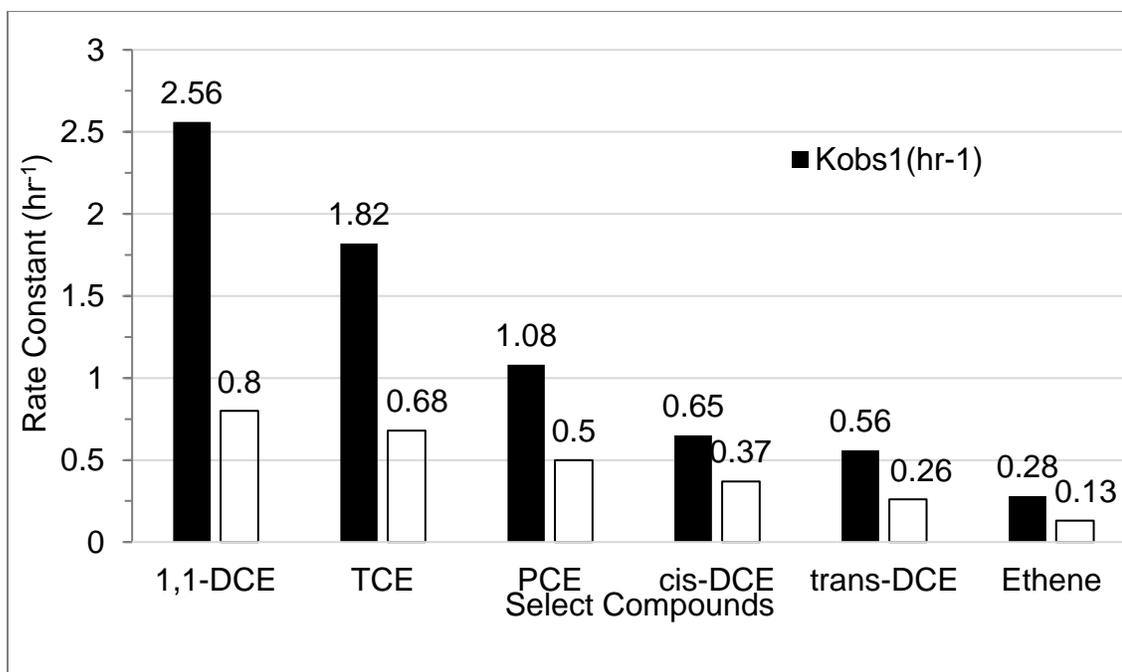
Figure 2.5: Comparison of k_{obs1} and k_{obs2} for studied compounds

Table 2.1: (A) k_{obs1} and k_{obs2} for *cis*-1,2-DCE for different ages of SD reduced HFO; (B) k_{obs1} and k_{obs2} for different initial amount of *cis*-1,2-DCE (C) k_{obs1} and k_{obs2} for *cis*-1,2-DCE for different molar ratio of HFO: SD; (D) k_{obs1} and k_{obs2} for studied compounds. Initial amount (μmol), R^2 of pseudo-first order fit and induction period (hr) are reported.

A. Effect of Aging (*cis*-1,2-DCE) (HFO:SD molar ratio 4.7:1)						
Age	Initial amount (μmol)	k_{obs1} (hr^{-1})	R^2	k_{obs2} (hr^{-1})	R^2	Induction period (hr)
3 hours	5.67	0.65	0.99	0.37	0.99	1.5
16 hours	5.47	0.65	0.99	0.37	0.99	0.5
7 days (302.4 hr)	5.51	0.64	0.98	0.26	0.99	1
B. Effect of Initial Amount (*cis*-1,2-DCE) (HFO:SD molar ratio 4.7:1; Age 16 hours)						
Initial amount (μmol)		k_{obs1} (hr^{-1})	R^2	k_{obs2} (hr^{-1})	R^2	Induction period (hr)
5.47		0.65	0.99	0.36	0.99	0.5
1.72		0.64	0.98	0.38	0.99	1
0.72		0.68	0.99	-	-	1
B. Effect of HFO: Dithionite Ratio (*cis*-1,2-DCE) (Age:16 hours)						
Ratio	Initial amount (μmol)	k_{obs1} (hr^{-1})	R^2	k_{obs2} (hr^{-1})	R^2	Induction period (hr)
2.4:1	5.34	0.78	1.00	0.47		2
4.7:1	5.47	0.65	0.99	0.37		0.5
9.4:1	5.68	0.06	0.98	0.01		>7
C. Select Compounds (Age: 16 hours; HFO:SD molar ratio 4.7:1)						
Select Compounds	Initial amount (μmol)	k_{obs1} (hr^{-1})	R^2	k_{obs2} (hr^{-1})	R^2	Induction period (hr)
1,1-DCE	2.26	2.56	1.00	0.80	0.98	1
TCE	0.38	1.82	0.97	0.68	0.97	0.5
PCE	0.035	1.08	0.99	0.50	0.97	1.5
cis-1,2-DCE	5.47	0.65	0.99	0.37	0.99	0.5
trans-1,2-DCE	5.46	0.56	1.00	0.26	1.00	1
Ethene	6.09	0.28	0.99	0.13	0.99	1

ADDITIONAL FIGURES
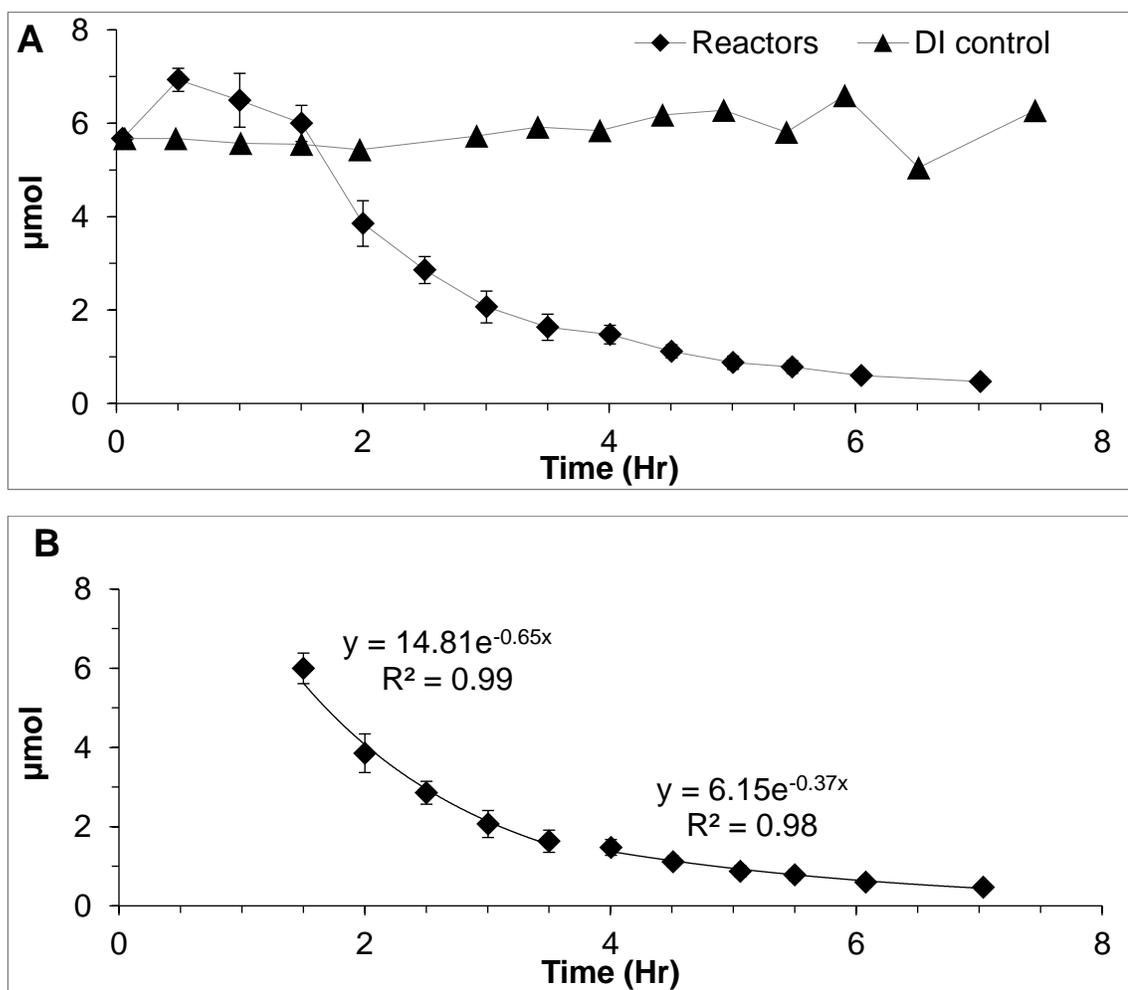
Figure 2.6: (A) *cis*-1,2-DCE degradation by oxygenation of SD reduced HFO aged for 3 hours. Experimental conditions: HFO:SD 4.7:1 molar ratio, 2 minutes oxygenation with pure oxygen; error bars indicate standard deviation among triplicate reactors (B) *cis*-1,2-DCE degradation rate constants: k_{obs1} and k_{obs2}
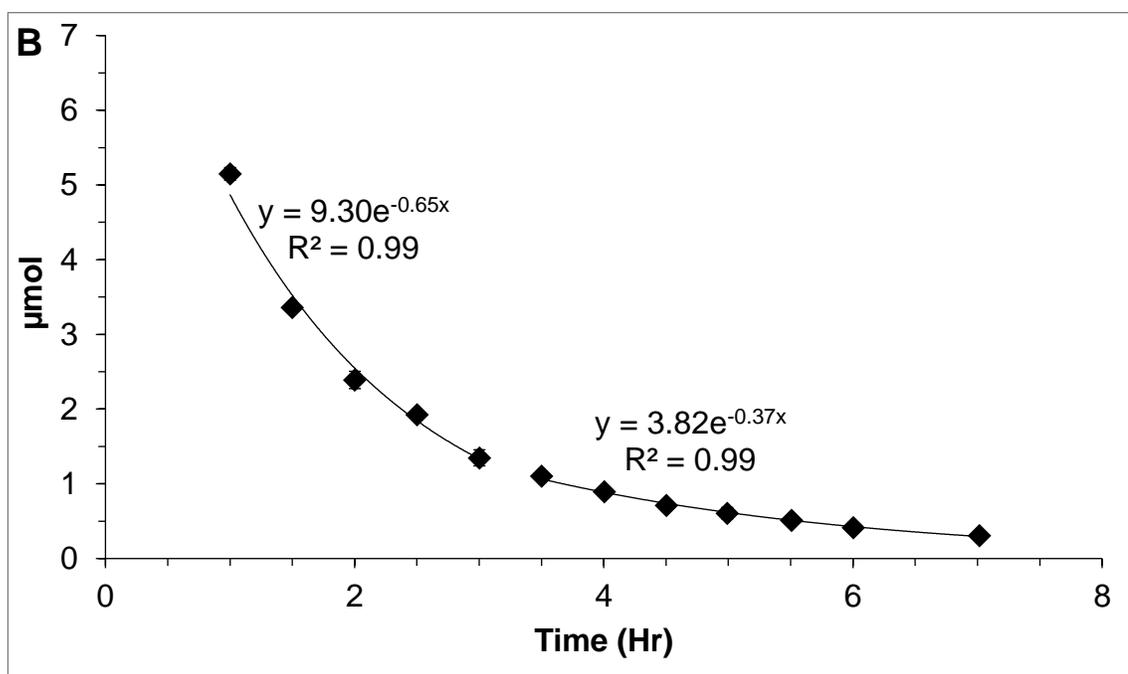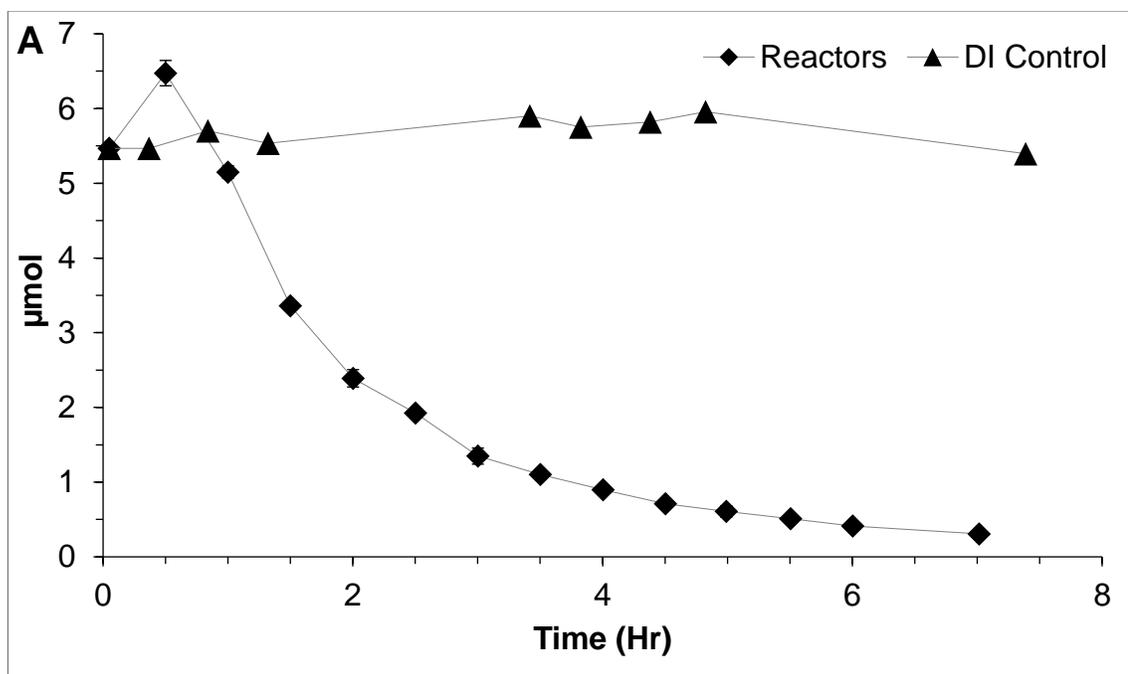
Figure 2.7: (A) *cis*-1,2-DCE degradation by oxygenation of SD reduced HFO aged for 16 hours. Experimental conditions: HFO:SD 4.7:1 molar ratio, 2 minutes oxygenation with pure oxygen; error bars indicate standard deviation among triplicate reactors (B) *cis*-1,2-DCE degradation rate constants: k_{obs1} and k_{obs2}
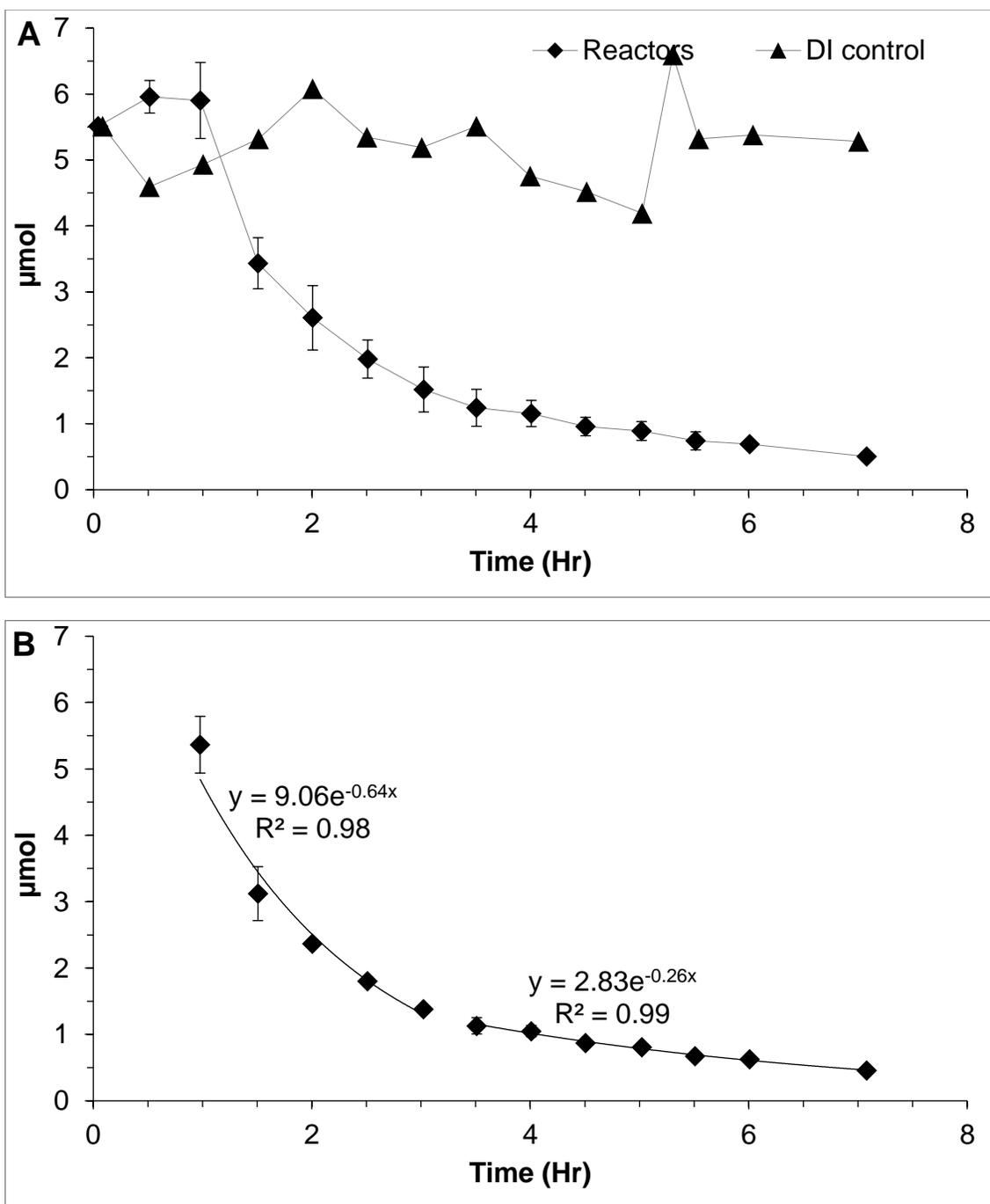
Figure 2.8: (A) *cis*-1,2-DCE degradation by oxygenation of SD reduced HFO aged for 7 days. Experimental conditions: HFO:SD 4.7:1 molar ratio, 2 minutes oxygenation with pure oxygen; error bars indicate standard deviation among triplicate reactors (B) *cis*-1,2-DCE degradation rate constants k_{obs1} and k_{obs2}
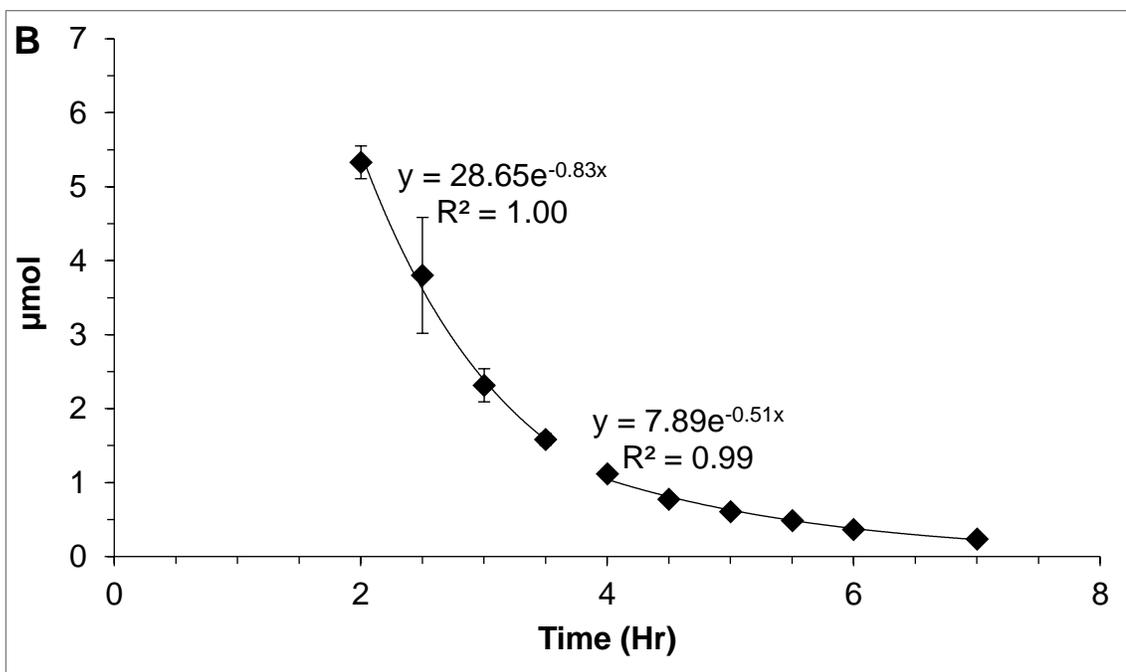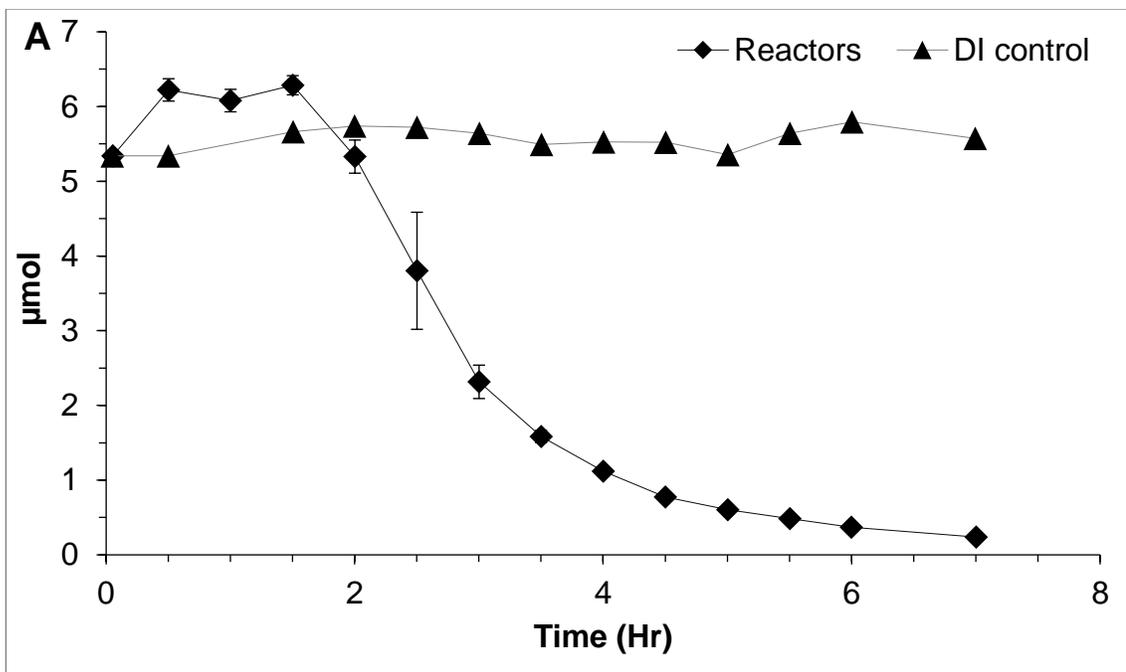
Figure 2.9: (A) *cis*-1,2-DCE degradation by oxygenation of SD reduced HFO (HFO:SD Molar ratio 2.4:1) Experimental conditions: 16 hours aging, 2 minutes oxygenation with pure oxygen; Error bars indicate standard deviation among triplicate reactors (B) *cis*-1,2-DCE degradation rate constants k_{obs1} and k_{obs2}
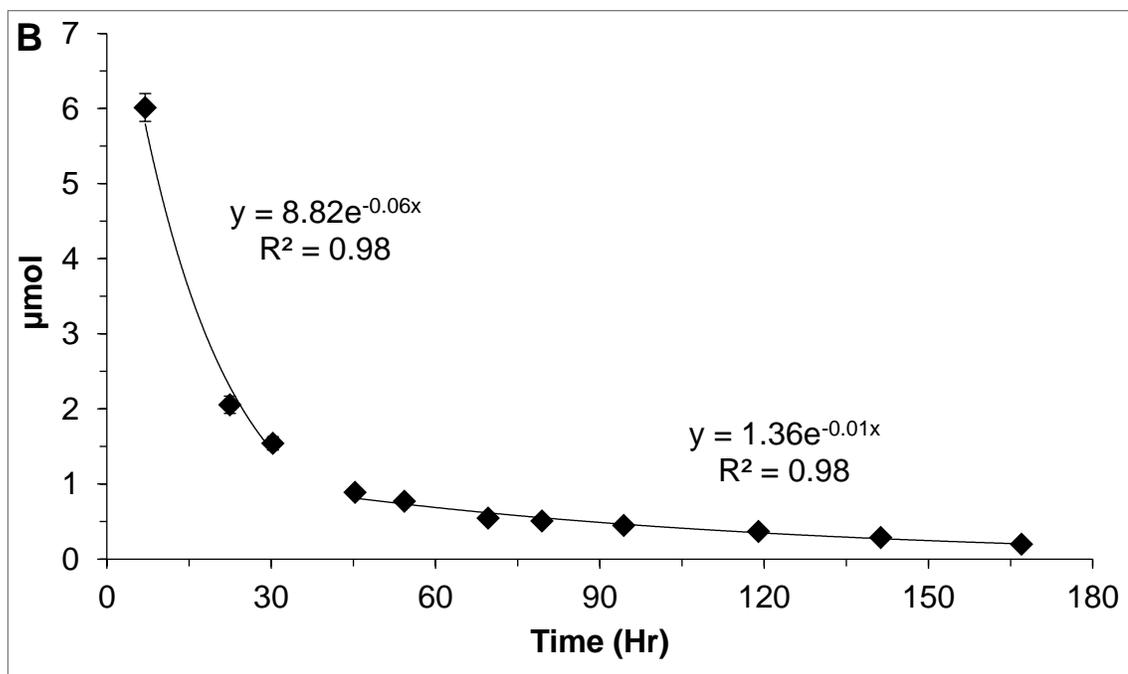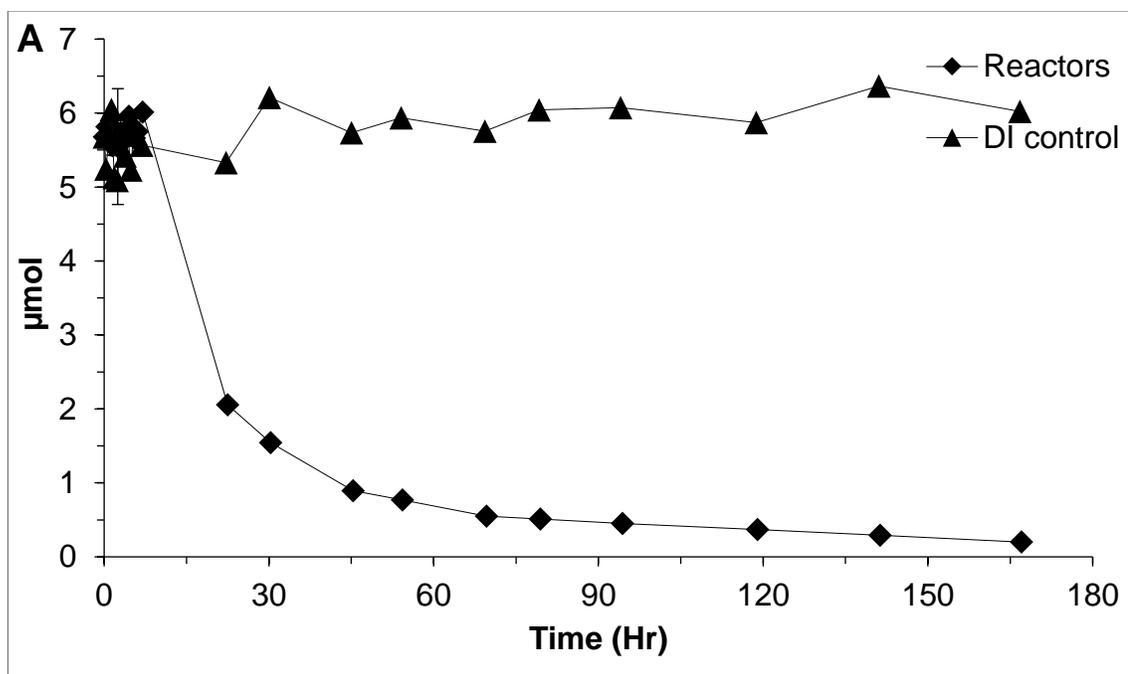
Figure 2.10: (A) *cis*-1,2-DCE degradation by oxygenation of SD reduced HFO (HFO:SD Molar ratio 9.4:1) Experimental conditions: 16 hours aging, 2 minutes oxygenation with pure oxygen; Error bars indicate standard deviation among triplicate reactors (B) *cis*-1,2-DCE degradation rate constants k_{obs1} and k_{obs}
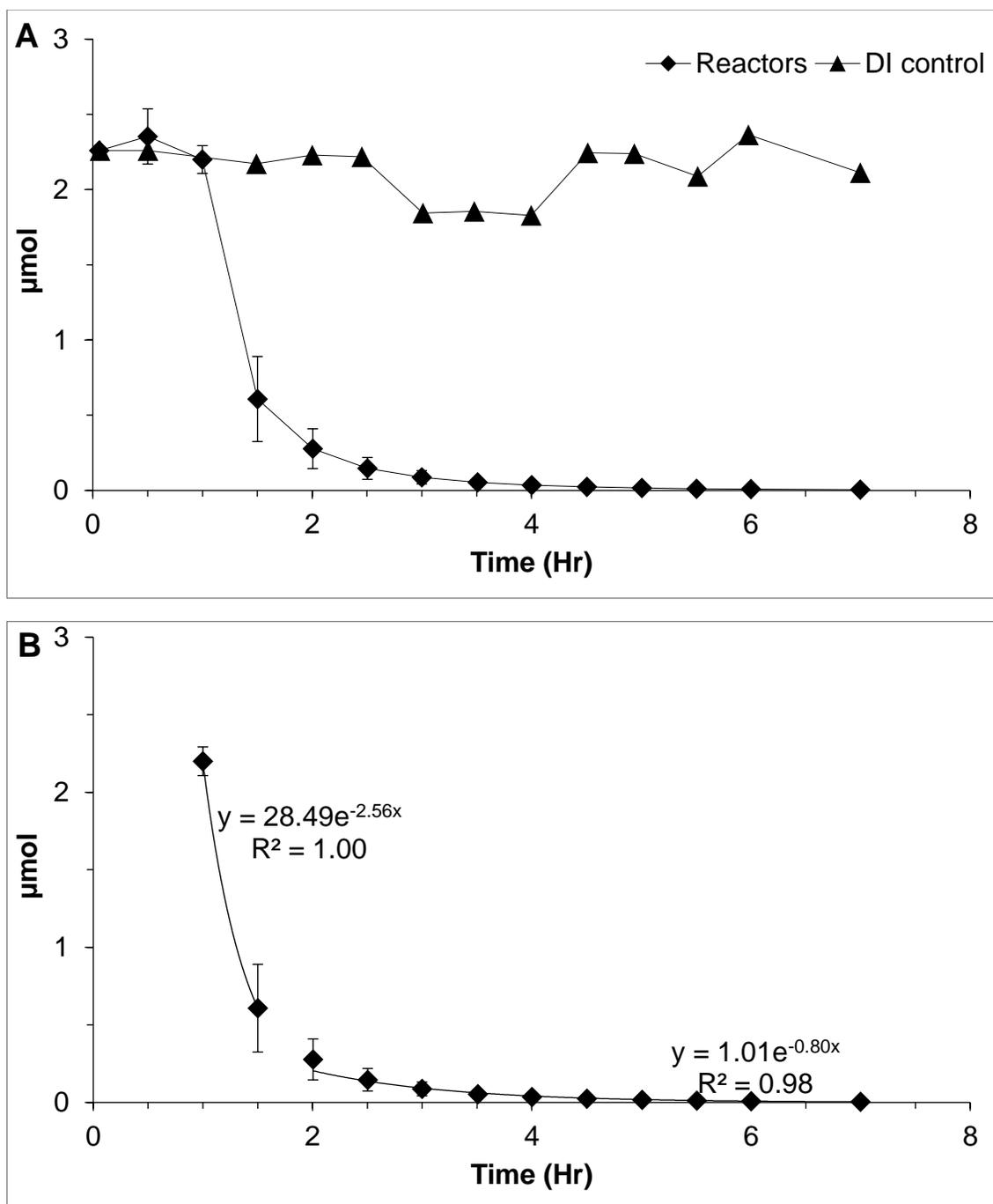
Figure 2.11: (A) 1,1-DCE degradation by oxygenation of SD reduced HFO. Experimental conditions: 16 hours aging, HFO:SD molar ratio 4.7:1, 2 minutes oxygenation with pure oxygen; Error bars indicate standard deviation among triplicate reactors (B) 1,1-DCE degradation rate constants k_{obs1} and k_{obs2}
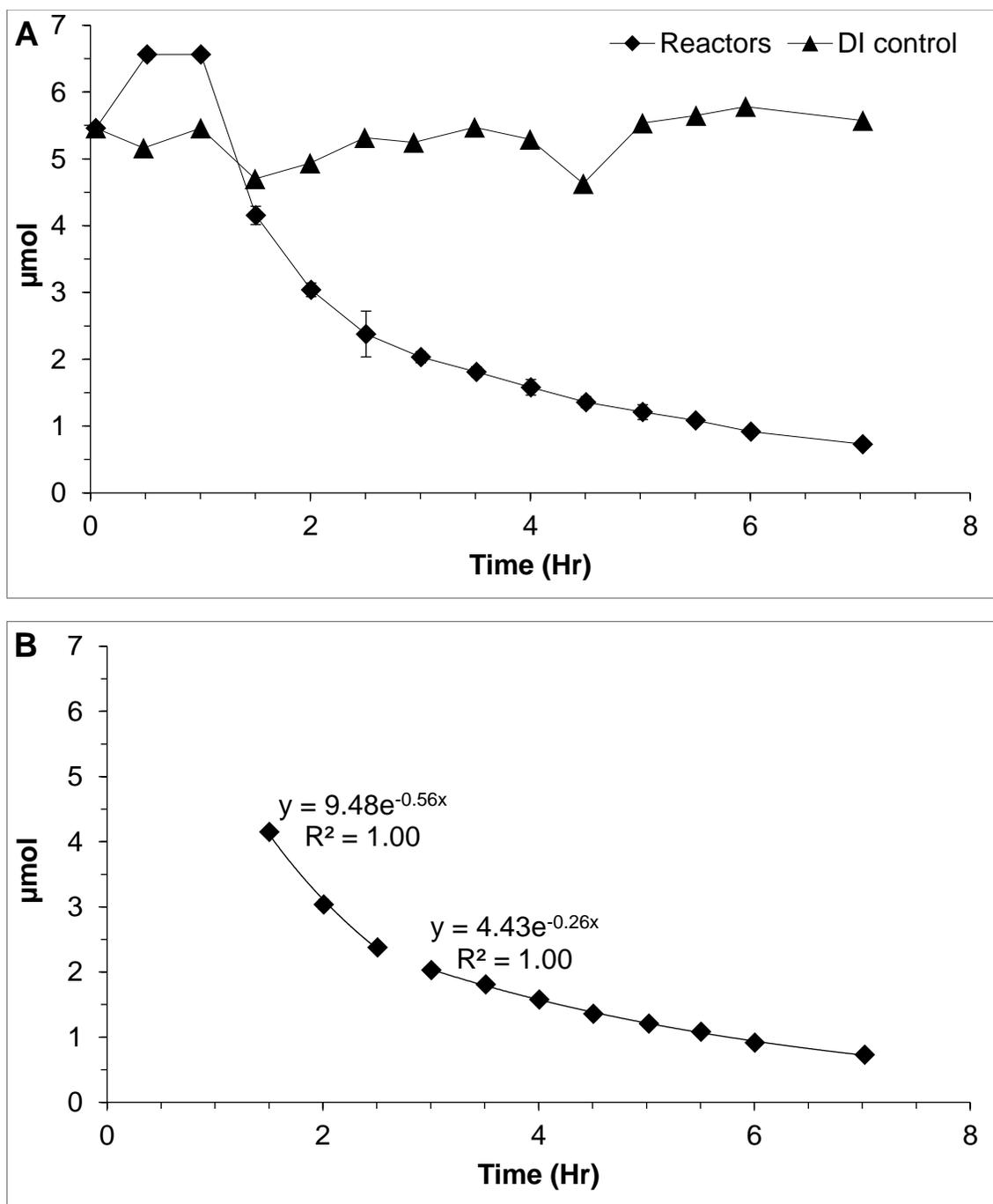
Figure 2.12: (A) *trans*-1,2-DCE degradation by oxygenation of SD reduced HFO. Experimental conditions: 16 hours aging, HFO:SD molar ratio 4.7:1, 2 minutes oxygenation with pure oxygen; Error bars indicate standard deviation among triplicate reactors (B) *trans*-1,2-DCE degradation rate constants k_{obs1} and k_{obs2}
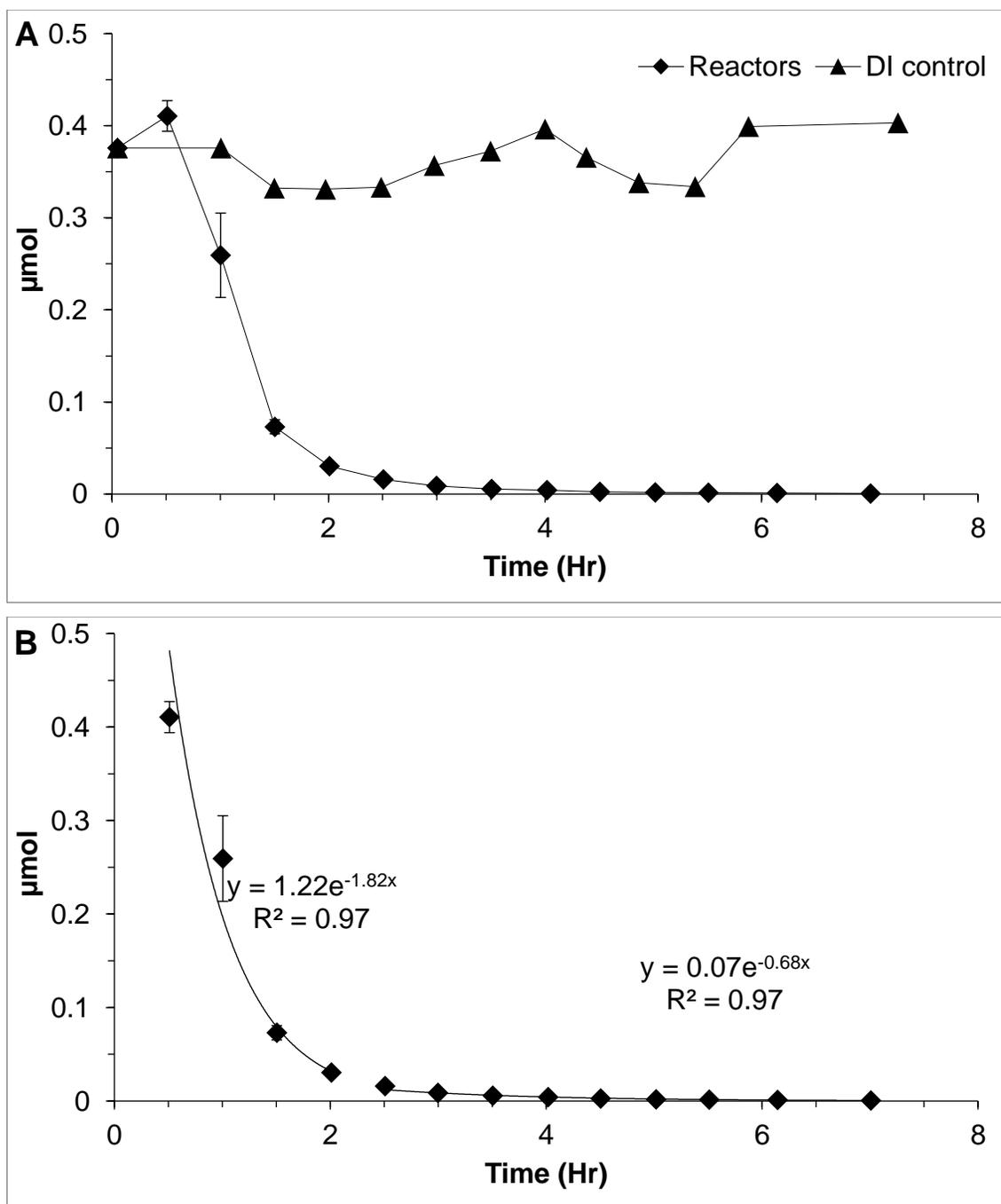
Figure 2.13: (A) TCE degradation by oxygenation of SD reduced HFO. Experimental conditions: 16 hours aging, HFO:SD molar ratio 4.7:1, 2 minutes oxygenation with pure oxygen; Error bars indicate standard deviation among triplicate reactors (B) TCE degradation rate constants k_{obs1} and k_{obs}
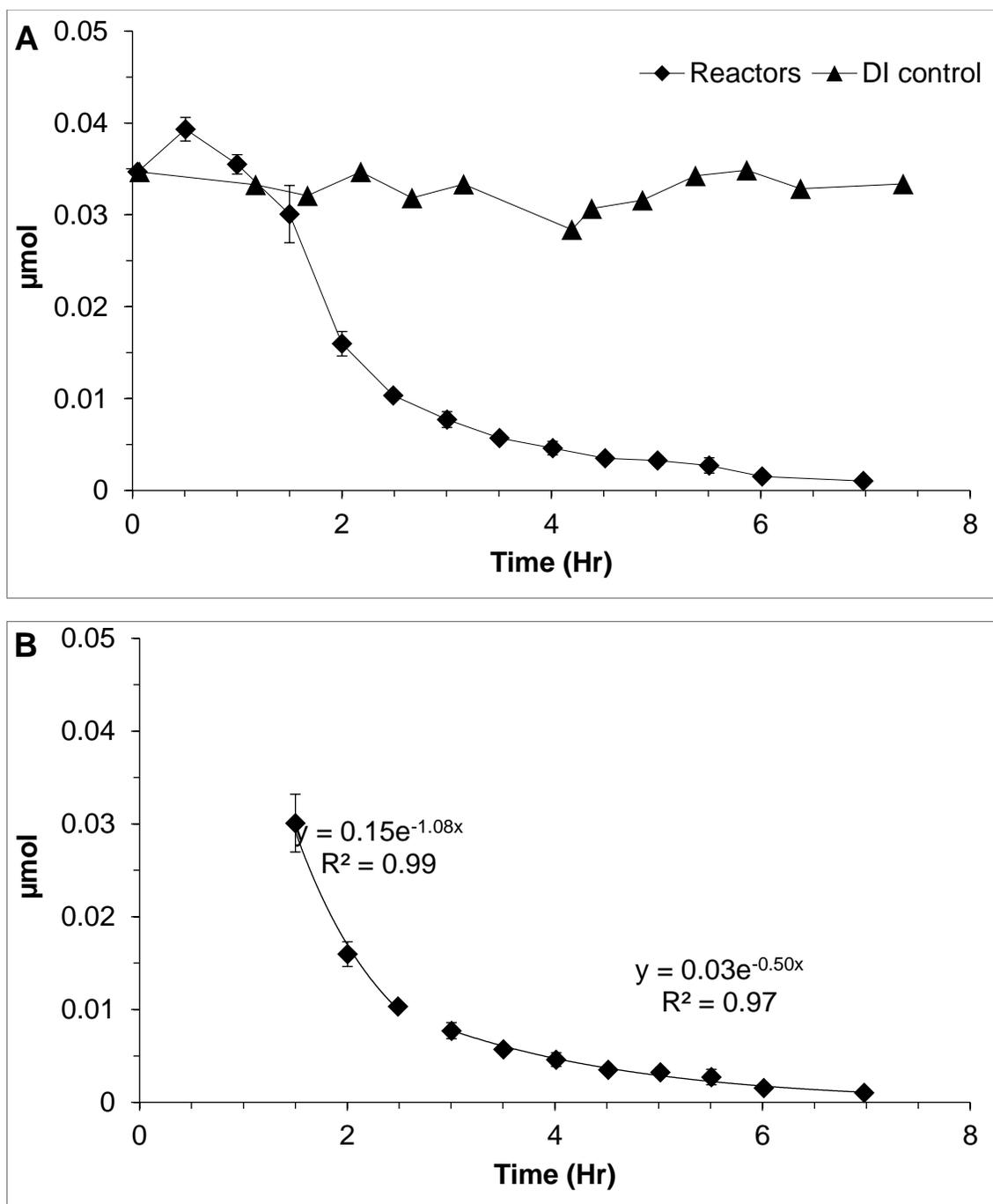
Figure 2.14: (A) PCE degradation by oxygenation of SD reduced HFO. Experimental conditions: 16 hours aging, HFO:SD molar ratio 4.7:1, 2 minutes oxygenation with pure oxygen; Error bars indicate standard deviation among triplicate reactors (B) PCE degradation rate constants k_{obs1} and k_{obs2}
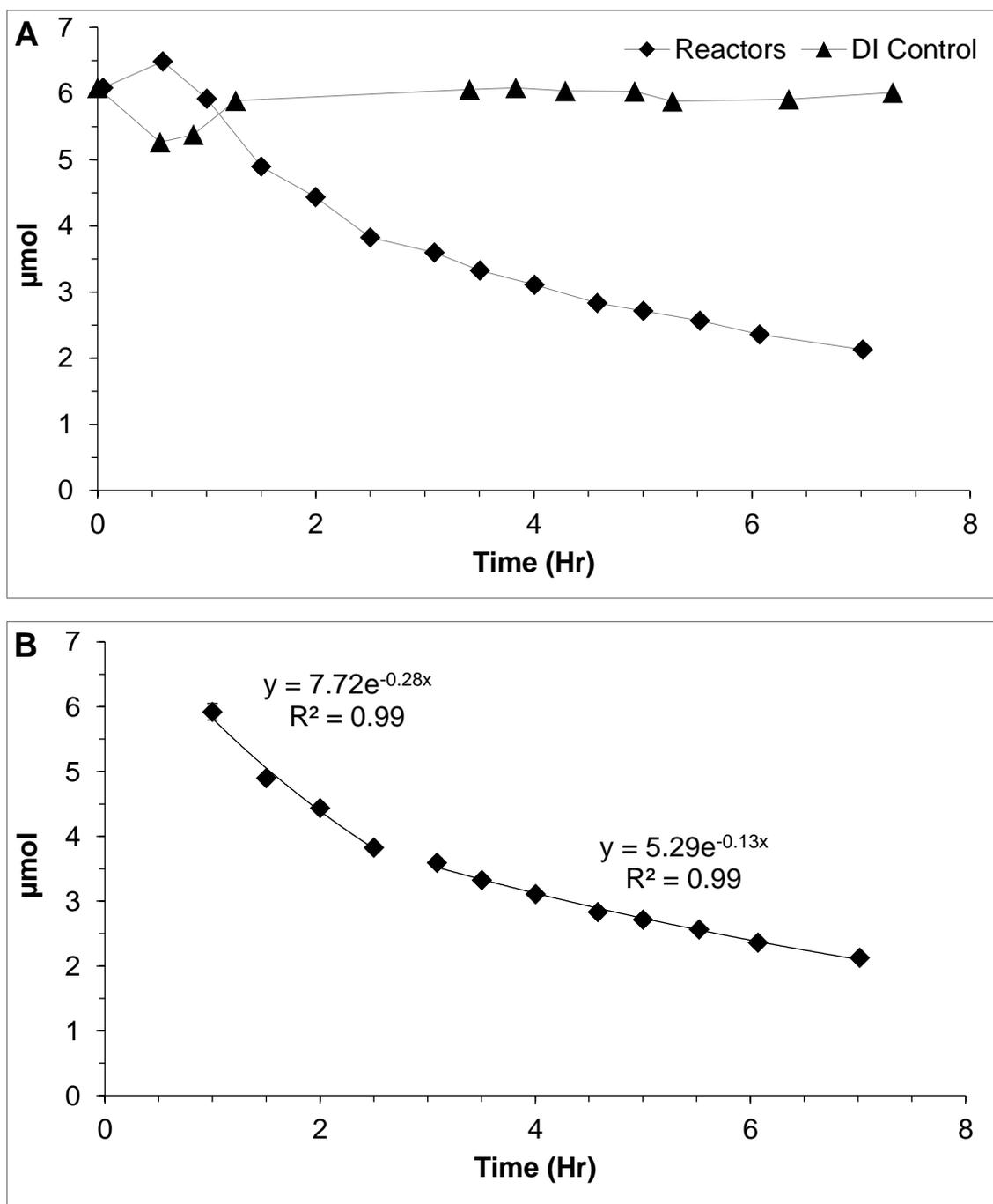
Figure 2.15: (A) Ethene degradation by oxygenation of SD reduced HFO. Experimental conditions: 16 hours aging, HFO:SD molar ratio 4.7:1, 2 minutes oxygenation with pure oxygen; Error bars indicate standard deviation among triplicate reactors (B) Ethene degradation rate constants k_{obs1} and k_{obs2}